

Compressible High-Speed Gas Flow

7

7.1 Introduction

Problems posed by high-speed gas flow are of obvious practical importance. Applications range from the *exterior flows* associated with flight to *interior flows* typical of turbomachinery. As the cost of physical experiments is high, the possibilities of computations were explored early and the development concentrated on the use of finite difference and associated finite volume methods. It was only in the 1980s that the potential offered by the finite element forms was realized and the field is expanding rapidly.

One of the main advantages in the use of the finite element approximation here is its capability of fitting complex forms and permitting local refinement where required. However, the improved approximation is also of substantial importance as practical problems will often involve three-dimensional discretization with the number of degrees of freedom much larger than those encountered in typical structural problems.

For such large problems direct solution methods are obviously not practicable and iterative methods based generally on transient computation forms are invariably used. Here of course we follow and accept much that has been established by the finite difference applications but generally will lose some computational efficiency associated with *structured meshes*. However, the reduction of the problem size which, as we shall see, can be obtained by local refinement and adaptivity will more than compensate for this loss (though of course structured meshes are included in the finite element forms).

In [Chapters 1](#) and [3](#) we introduced the basic equations governing the flow of compressible gases as well as of incompressible fluids. Indeed in the latter, as in [Chapter 4](#), we can introduce small amounts of compressibility into the procedures developed there specifically for incompressible flow. In this chapter we shall deal with high-speed flows. Such flows will usually involve the formation of shocks with characteristic discontinuities. For this reason we shall concentrate on the use of low-order elements and explicit methods, such as those introduced in [Chapters 2](#) and [3](#).

Here the pioneering work of the author's colleagues Morgan, Löhner, Peraire, Hassan, and Weatherill must be acknowledged [[1–48](#)]. It was this work that opened the doors to practical finite element analysis in the field of aeronautics. We shall refer to their work frequently.

In the first practical applications the Taylor-Galerkin process outlined in [Appendix D](#) for vector-valued variables was used almost exclusively. Here we recommend however the CBS algorithm discussed in [Chapter 3](#) as it presents a better approximation and has the advantage of dealing directly with incompressibility, which invariably occurs in small parts of the domain, even at high Mach numbers (e.g., in stagnation regions).

7.2 The governing equations

The Navier-Stokes governing equations for compressible flow were derived in [Chapter 1](#). We shall repeat only the simplified form of [Eq. \(1.25\)](#) here again using indicial notation. We thus write, for $i = 1, 2, 3$,

$$\frac{\partial \Phi}{\partial t} + \frac{\partial \mathbf{F}_i}{\partial x_i} + \frac{\partial \mathbf{G}_i}{\partial x_i} + \mathbf{Q} = \mathbf{0} \quad (7.1)$$

with

$$\Phi = [\rho, \rho u_1, \rho u_2, \rho u_3, \rho E]^T \quad (7.2a)$$

$$\mathbf{F}_i = [\rho u_i, \rho u_1 u_i + p \delta_{1i}, \rho u_2 u_i + p \delta_{2i}, \rho u_3 u_i + p \delta_{3i}, \rho H u_i]^T \quad (7.2b)$$

$$\mathbf{G}_i = \left[0, -\tau_{1i}, -\tau_{2i}, -\tau_{3i}, -\frac{\partial}{\partial x_i}(\tau_{ij} u_j) - k \left(\frac{\partial T}{\partial x_i} \right) \right]^T \quad (7.2c)$$

and

$$\mathbf{Q} = [0, -\rho f_1, -\rho f_2, -\rho f_3, -\rho f_i u_i - q_H]^T \quad (7.2d)$$

In the above

$$\tau_{ij} = \mu \left[\left(\frac{\partial u_i}{\partial x_j} + \frac{\partial u_j}{\partial x_i} \right) - \delta_{ij} \frac{2}{3} \frac{\partial u_k}{\partial x_k} \right] \quad (7.2e)$$

The above equations need to be “closed” by addition of the constitutive law relating the pressure, density, and energy (see [Chapter 1](#)). For many flows the ideal gas law [[49](#)] suffices and this is

$$\rho = \frac{p}{RT} \quad (7.3)$$

where R is the universal gas constant. In terms of specific heats

$$R = (c_p - c_v) = (\gamma - 1)c_v \quad (7.4)$$

where

$$\gamma = \frac{c_p}{c_v}$$

is the ratio of the constant pressure and constant volume-specific heats.

The internal energy e and total specific energy E are given as

$$\begin{aligned} e &= c_v T = \left(\frac{1}{\gamma - 1} \right) \frac{p}{\rho} \\ E &= e + \frac{1}{2} u_i u_i \end{aligned} \quad (7.5)$$

and hence

$$\rho E = \left(\frac{1}{\gamma - 1} \right) p + \rho \frac{u_i u_i}{2} \quad (7.6a)$$

$$\rho H = \rho E + p = \left(\frac{\gamma}{\gamma - 1} \right) p + \rho \frac{u_i u_i}{2} \quad (7.6b)$$

The variables for which we shall solve are usually taken as the set of Eq. (7.2a), i.e.

$$\rho, \rho u_i, \text{ and } \rho E$$

but of course other sets could be used, though then the conservative form of Eq. (7.1) could be lost.

In many of the problems discussed in this chapter inviscid behavior will be assumed, with

$$\mathbf{G}_i = \mathbf{0}$$

and we shall then deal with the *Euler equations*.

In many problems the Euler solution will provide information about the main features of the flow and will suffice for many purposes, especially if augmented by separate boundary layer calculations (see Section 7.13). However, in principle it is possible to include the viscous effects without much apparent complication. Here in general steady-state conditions will never arise as the high speed of the flow will be associated with turbulence and this will usually be of a small scale capable of resolution with very small-sized elements only. If a “finite” size of element mesh is used then such turbulence will often be suppressed and steady-state answers will be obtained. We shall in some examples include such full Navier-Stokes solutions using a viscosity dependent on the temperature according to Sutherland’s law [49]. In the SI system of units for air this gives

$$\mu = \frac{1.45 T^{3/2}}{T + 110} \times 10^{-6} \quad (7.7)$$

where T is in Kelvin. Further turbulence modeling can be done by using the Reynolds-averaged equations and solving additional transport equations for some additional parameters in the manner discussed in Chapter 8.

7.3 Boundary conditions: Subsonic and supersonic flow

The question of boundary conditions which can be prescribed for Euler and Navier-Stokes equations in compressible flow is by no means trivial and has been addressed in

a general sense by Demkowicz et al. [50], determining their influence on the existence and uniqueness of solutions. In the following we shall discuss the case of the inviscid Euler form and of the full Navier-Stokes problem.

We have already discussed the general question of boundary conditions in Chapter 3 dealing with numerical approximations. Some of these matters have to be repeated in view of the special behavior of high-speed flow problems.

7.3.1 Euler equation

Here only first-order derivatives occur and the number of boundary conditions is less than that for the full Navier-Stokes problem.

For a *solid wall boundary*, Γ_u , only the normal component of velocity u_n needs to be specified (zero if the wall is stationary). Further, with lack of conductivity the energy flux across the boundary is zero and hence ρE (and ρ) remain unspecified.

In general the analysis domain will be limited by some arbitrarily chosen *external boundaries*, Γ_s , for exterior or internal flows, as shown in Fig. 7.1 (see also Section 3.9, Chapter 3).

Here, it will in general be necessary to perform a linearized Riemann analysis in the direction of the outward normal to the boundary \mathbf{n} to determine the speeds of wave propagation of the equations. For this linearization of the Euler equations three propagation speed values (characteristics) can be found in one dimension (eigenvalues of the Jacobian matrix) [49, 51]:

$$\begin{aligned} c_o &= u_n \\ c_+ &= u_n + c \\ c_- &= u_n - c \end{aligned} \quad (7.8)$$

where u_n is the normal velocity component and c is the compressible wave celerity (speed of sound) given by

$$c = \sqrt{\frac{\gamma p}{\rho}} \quad (7.9)$$

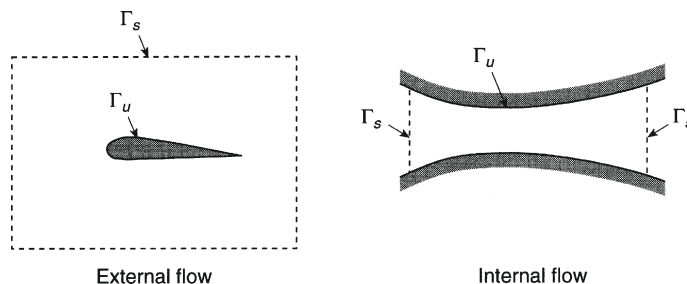


FIGURE 7.1

Boundaries of a computation domain. Γ_u , wall boundary; Γ_s , fictitious boundary.

As of course no disturbances can propagate at velocities greater than those of Eq. (7.8) in the case of supersonic flow, i.e., when the local Mach number is

$$M = \frac{|u_n|}{c} \geq 1 \quad (7.10)$$

we shall have to distinguish two possibilities:

- (a) *Supersonic inflow boundary* where

$$u_n > c$$

and the analysis domain cannot influence the upstream position (all characteristics are directed into the domain at the inlet); for such boundaries all components of the vector Φ must be specified.

- (b) *Supersonic outflow boundaries* where

$$u_n > c$$

and here by the same reasoning no components of Φ are prescribed (all characteristics are directed out of the domain).

For subsonic boundaries the situation is more complex and here the values of Φ that can be specified are the components of the incoming Riemann variables. However, this may frequently present difficulties as the incoming wave may not be known and the usual compromises may be necessary as in the treatment of elliptic problems possessing infinite boundaries (see Chapter 3, Section 3.9).

It is often convenient to prescribe boundary conditions for a subsonic flow by once again considering the direction of characteristics from Eq. (7.8). Since $u_n < c$ in subsonic flows, one characteristic at the inlet will be directed outwards and two will be directed inwards. At the exit one characteristic is directed inward and two outwards as shown in Figure 7.2. Thus, it is necessary to prescribe two boundary conditions at the inlet and one at the exit for the subsonic condition shown in Figure 7.2. However, this procedure is not easy to follow in multidimensional problems.

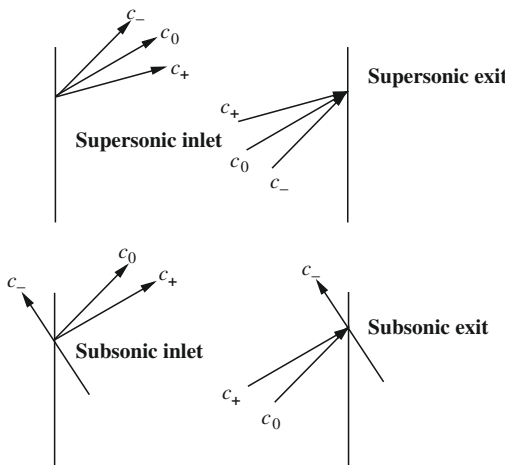
7.3.2 Navier-Stokes equations

Here, due to the presence of second derivatives, additional boundary conditions are required.

For the *solid wall boundary*, Γ_u , all the velocity components are prescribed assuming, as in the previous chapter for incompressible flow, that the fluid is attached to the wall. Thus for a stationary boundary we put

$$u_i = 0$$

Further, if conductivity is not negligible, boundary temperatures or heat fluxes will generally be given in the usual manner.

**FIGURE 7.2**

Characteristic directions at inlet and exit for supersonic and subsonic flows.

For exterior boundaries Γ_s of the supersonic inflow kind, the treatment is identical to that used for Euler equations. However, for outflow boundaries a further approximation must be made, either specifying tractions as zero or making their gradient zero in the manner described in [Section 3.9, Chapter 3](#).

7.4 Numerical approximations and the CBS algorithm

Various forms of finite element approximation and of solution have been used for compressible flow problems. The first successfully used algorithm here was, as we have already mentioned, the Taylor-Galerkin procedure either in its single-step or two-step form. We have outlined both of these algorithms in [Appendix D](#). However, the most generally applicable and advantageous form is that of the CBS algorithm which we have presented in detail in [Chapter 3](#). In all compressible flows in certain parts of the domain where the velocities are small, the flow is nearly incompressible and without additional damping the direct use of the Taylor-Galerkin method may result in oscillations there. We indeed mentioned an example of such oscillations in [Chapter 3](#) where they are pronounced near the leading edge of an aerofoil even at quite high Mach numbers ([Fig 3.4](#)). With the use of the CBS algorithm such oscillations disappear and the solution is perfectly stable and accurate.

In the same example we also discussed the single-step and two-step forms of the CBS algorithm. We recommend the two-step procedure, which is only slightly more expensive than the single-step version but more stable.

As we have already remarked if the algorithm is used for steady-state problems it is always convenient to use a localized time step rather than proceed with the same

time step globally. The full description of the local time step procedure is given in [Section 3.4.4](#) of [Chapter 3](#) and this was invariably used in the examples of this chapter when only the steady state was considered. We now summarize the explicit solution procedure below:

```

do i = 1,number of time steps
    step1: calculation of intermediate momentum
    step2: calculation of density
    step3: correction of momentum
    step4: energy equation
    step5: pressure calculation from energy and density
  enddo !i

```

For further details on the algorithm, readers are referred to [Chapter 3](#). If shock capturing or any other form of smoothing is found necessary this is integrated into the first step of the above solution procedure.

One of the additional problems that we need to discuss further for compressible flows is that of the treatment of shocks, which is the subject of the next section.

7.5 Shock capture

Clearly with the finite element approximation in which all the variables are interpolated using C_0 continuity the exact reproduction of shocks is not possible. In all finite element solutions we therefore represent the shocks simply as regions of very high gradient. The ideal situation will be if the rapid variations of variables are confined to a few elements surrounding the shock. Unfortunately it will generally be found that such an approximation of a discontinuity introduces local oscillations and these may persist throughout quite a large area of the domain. For this reason, we shall usually introduce into the finite element analysis additional viscosities which will help us in damping out any oscillations caused by shocks and, yet, deriving as sharp a solution as possible.

Such procedures using artificial viscosities are known as shock capture methods. It must be mentioned that some investigators have tried to allow the shock discontinuity to occur explicitly and thus allowed a discontinuous variation of an analytically defined kind. This presents very large computational difficulties and it can be said that to date such trials have only been limited to one-dimensional problems and have not really been used to any extent in two or three dimensions. For this reason we shall not discuss such *shock fitting* methods further [[52,53](#)].

The concept of adding additional viscosity or diffusion to capture shocks was first suggested by von Neumann and Richtmyer [[54](#)] as early as 1950. They recommended that stabilization can be achieved by adding a suitable artificial dissipation term that mimics the action of viscosity in the neighborhood of shocks. Significant developments in this area are those of Lapidus [[55](#)], Steger [[56](#)], MacCormack and Baldwin [[57](#)], and Jameson and Schmidt [[58](#)]. At Swansea, a modified form of the method based on the second derivative of pressure has been developed by Peraire et al. [[14](#)]

and Morgan et al. [59] for finite element computations. This modified form of viscosity with a pressure switch calculated from the nodal pressure values is used subsequently in compressible flow calculations. Lately an anisotropic viscosity for shock capturing [60] has been introduced to add diffusion in a more rational way.

The implementation of artificial diffusion is very much simpler than shock fitting and we proceed as follows. In this we first calculate the approximate quantities of the solution vector by using the direct explicit method. Now we modify each scalar component of these quantities by adding a correction which smoothes the result. Thus for instance if we consider a typical scalar component quantity ϕ and have determined the values of ϕ^{n+1} , we establish the new values as below:

$$\phi_s^{n+1} = \phi^{n+1} + \Delta t \mu_a \frac{\partial}{\partial x_i} \left(\frac{\partial \phi}{\partial x_i} \right) \quad (7.11)$$

where μ_a is an appropriate artificial diffusion coefficient. It is important that whatever the method used, the calculation of μ_a should be limited to the domain which is close to the shock as we do not wish to distort the results throughout the problem. For this reason many procedures add a *switch* usually activated by such quantities as gradients of pressure. In all of the procedures used we can write the quantity μ_a as a function of one or more of the dependent variables calculated at time n . Below we only quote two of the possibilities.

7.5.1 Second derivative-based methods

In these it is generally assumed that the coefficient μ_a must be the same for each of the equations dealt with and only one of the dependent variables Φ is important. It has usually been assumed that the most typical variable here is the pressure and that we should write [57]

$$\mu_a = C_e h^3 \frac{|\mathbf{u}| + c}{\bar{p}} \left| \frac{\partial^2 p}{\partial x_i \partial x_i} \right|_e \quad (7.12)$$

where C_e is a nondimensional coefficient, \mathbf{u} is the velocity vector, c is the speed of sound, \bar{p} is the average pressure, and the subscript e indicates an element. In the above equation, the second derivative of pressure over an element can be established either by averaging the smoothed nodal pressure gradients or using any of the methods described in Chapter 4, Section 4.3.3.

A particular variant of the above method evaluates approximately the value of the second derivative of any scalar variable ϕ (e.g., p) as [59, 61]

$$h^2 \overline{\frac{\partial^2 \phi}{\partial x^2}} \approx (\mathbf{M} - \mathbf{M}_L) \tilde{\phi} \quad (7.13)$$

where \mathbf{M} and \mathbf{M}_L are consistent and lumped mass matrices respectively and the tilde indicates a nodal value. Though the derivation of the above expression is not obvious, the reader can verify that in the one-dimensional finite difference approximation

it gives the correct result. The heuristic extension to multidimensional problem therefore seems reasonable. Now μ_a for this approximate method can be rewritten in any space dimensions as [Eq. (7.12)]

$$\tilde{\mu}_a = C_e h \frac{|\mathbf{u}| + c}{\bar{p}} (\mathbf{M} - \mathbf{M}_L) \tilde{\mathbf{p}} \quad (7.14)$$

Note now that $\tilde{\mu}_a$ is a nodal quantity. However a further approximation can give the following form of μ_a over elements:

$$\mu_{ae} = C_e h (|\mathbf{u}| + c) S_e \quad (7.15)$$

where S_e is the element pressure switch which is a mean of nodal switches S_i calculated as [59, 61]

$$S_i = \frac{|\Sigma_e(p_i - p_k)|}{\Sigma_e|p_i - p_k|} \quad (7.16)$$

It can be verified that $S_i = 1$ when the pressure has a local extremum at node i and $S_i = 0$ when the pressure at node i is the average of the values for all nodes adjacent to node i (e.g., if p varies linearly). The user-specified coefficient C_e normally varies between 0.0 and 2.0.

The smoothed variables can now be rewritten with the Galerkin finite element approximations [from Eqs. (7.11) and (7.15)] as

$$\tilde{\phi}_s^{n+1} = \tilde{\phi}^{n+1} + \Delta t \mathbf{M}_L^{-1} \frac{C_e S_e}{\Delta t_e} (\mathbf{M} - \mathbf{M}_L) \tilde{\phi}^n \quad (7.17)$$

Note that, in Eq. (7.15), $(|\mathbf{u}| + c)$ is replaced by $h/\Delta t_e$ to obtain the above equation. This method has been widely used and is very efficient. The cutoff localizing the effect of added diffusion is quite sharp. A direct use of second derivatives can however be employed without the above-mentioned modifications. In such a procedure, we have the following form of smoothing [from Eqs. (7.11) and (7.12)]:

$$\tilde{\phi}_s^{n+1} = \tilde{\phi}^{n+1} - \Delta t \mathbf{M}_L^{-1} C_e h^3 \frac{|\mathbf{u}| + c}{\bar{p}} \left| \frac{\partial^2 p}{\partial x_i^2} \right|_e \left(\int_{\Omega} \frac{\partial \mathbf{N}^T}{\partial x_i} \frac{\partial \mathbf{N}}{\partial x_i} \tilde{\phi}^n d\Omega \right) \tilde{\phi}^n \quad (7.18)$$

This method was successful in many viscous problems. Another alternative is to use residual-based methods.

7.5.2 Residual-based methods

In these methods $\mu_{ai} = \mu(R_i)$, where R_i is the residual of the i th equation. Such methods were first introduced in 1986 by Hughes and Malett [62] and later used by many others [63–66].

A variant of this was suggested by Codina [60]. We sometimes refer to this as anisotropic shock capturing. In this procedure the artificial viscosity coefficient is

adjusted by subtracting the diffusion introduced by the characteristic-Galerkin method along the streamlines. We do not know whether there is any advantage gained in this but we have used the anisotropic shock capturing algorithm with considerable success. The full residual-based coefficient is given by

$$\mu_{a_i} = C_e \frac{|R_i|}{|\nabla \phi_i|} \quad (7.19)$$

We shall not discuss here a direct comparison between the results obtained by different shock capturing diffusivities, and the reader is referred to various papers already published [61, 67]. Another smoothing procedure occasionally used in low Mach number flows is referred to as “variable smoothing” and this method is discussed in the following section.

7.6 Variable smoothing

At low Mach numbers, we found it often necessary to include a variable smoothing procedure if the coupling between the energy and other variables exists. Of course isothermal approximations are possible to get a smooth solution. However, to solve a compressible flow problem at low Mach numbers (< 0.8) without removing energy coupling we recommend a variable smoothing approach [68]. In the proposed variable smoothing approach the conservation variables, $\{\Phi\}$, at a node are smoothed by applying the following redistribution:

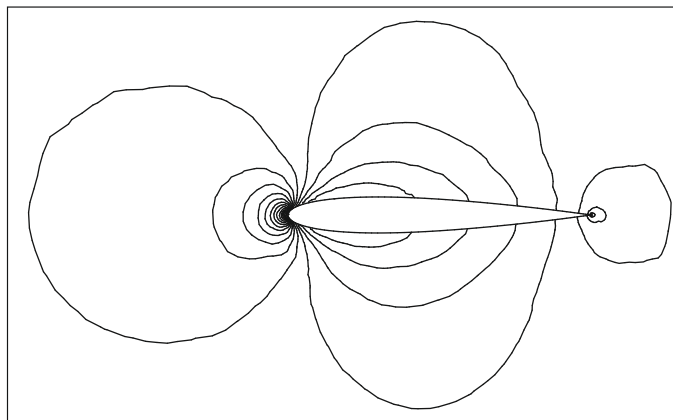
$$\{\Phi\} = \left[\frac{1}{1 + 0.5\alpha} \{\Phi\} + \frac{\alpha}{1 + 0.5\alpha} \mathbf{M}_L^{-1} (\mathbf{M} - \mathbf{M}_D) \{\Phi\} \right] \quad (7.20)$$

where α is a variable smoothing parameter which varies between 0 and 0.05, \mathbf{M} is the consistent mass matrix, \mathbf{M}_D is the consistent mass matrix without nondiagonal terms, and \mathbf{M}_L is the lumped mass matrix. By increasing α the weighting on the node in question is decreased while the influence of the surrounding nodes is increased. In [Figure 7.3](#) we show the smoothed density contours of subsonic flow past a NACA0012 airfoil at a Mach number of 0.25. The results without smoothing give a very oscillatory solution as shown in [Figure 7.4](#) in which the pressure coefficients from smoothed and unsmoothed solutions are compared.

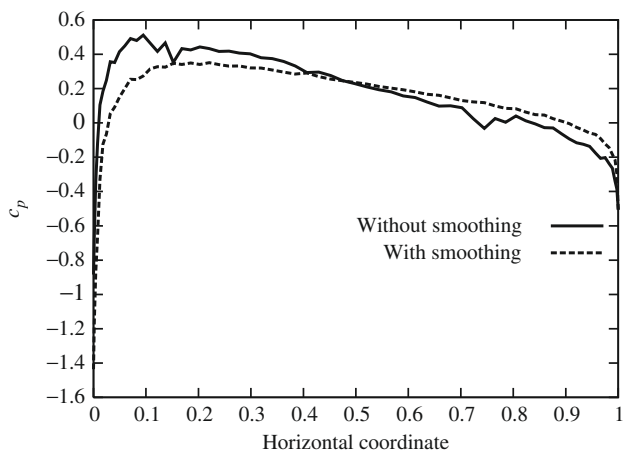
At transonic and supersonic speeds, an additional shock capturing dissipation ([Section 7.5](#)) is necessary to capture and to smooth local oscillations in the vicinity of shocks.

7.7 Some preliminary examples for the Euler equation

The computation procedures outlined can be applied with success to many transient and steady-state problems. In this section we illustrate its performance on a few relatively simple examples.

**FIGURE 7.3**

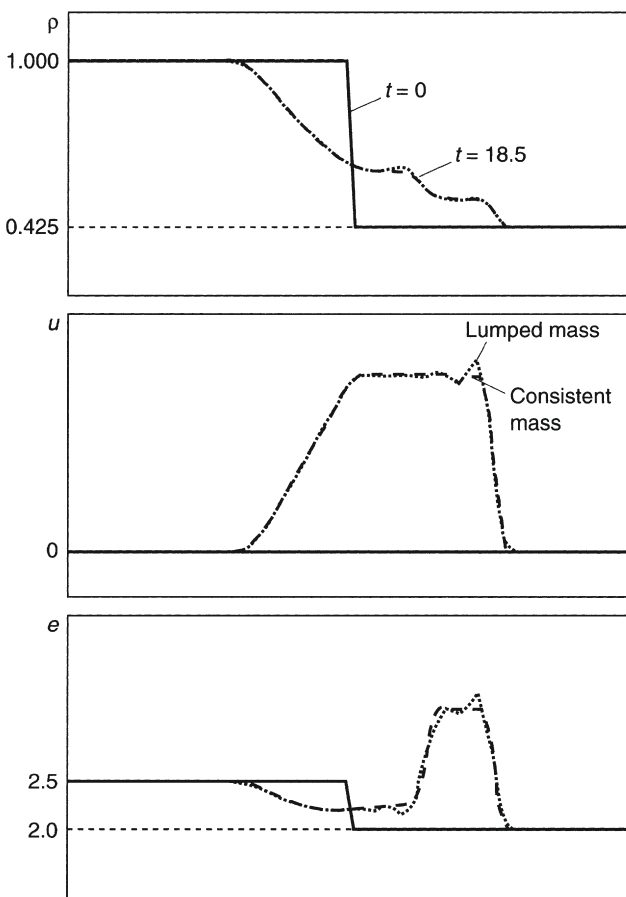
Subsonic inviscid flow past a NACA0012 airfoil at Mach number of 0.25 and zero angle of attack. Smoothed density contours [68].

**FIGURE 7.4**

Subsonic inviscid flow past a NACA0012 airfoil at Mach number of 0.25 and zero angle of attack. Comparison between smoothed and unsmoothed pressure coefficients [68].

Example 7.1. Riemann shock tube: A transient problem in one dimension

This is treated as a one-dimensional problem. Here an initial pressure difference between two sections of the tube is maintained by a diaphragm which is destroyed at $t = 0$. Figure 7.5 shows the pressure, velocity, and energy contours at the 70th time increment, and the effect of including consistent and lumped mass matrices is illustrated. The problem has an analytical, exact, solution presented by Sod [69] and the numerical solution is from Ref. [1].

**FIGURE 7.5**

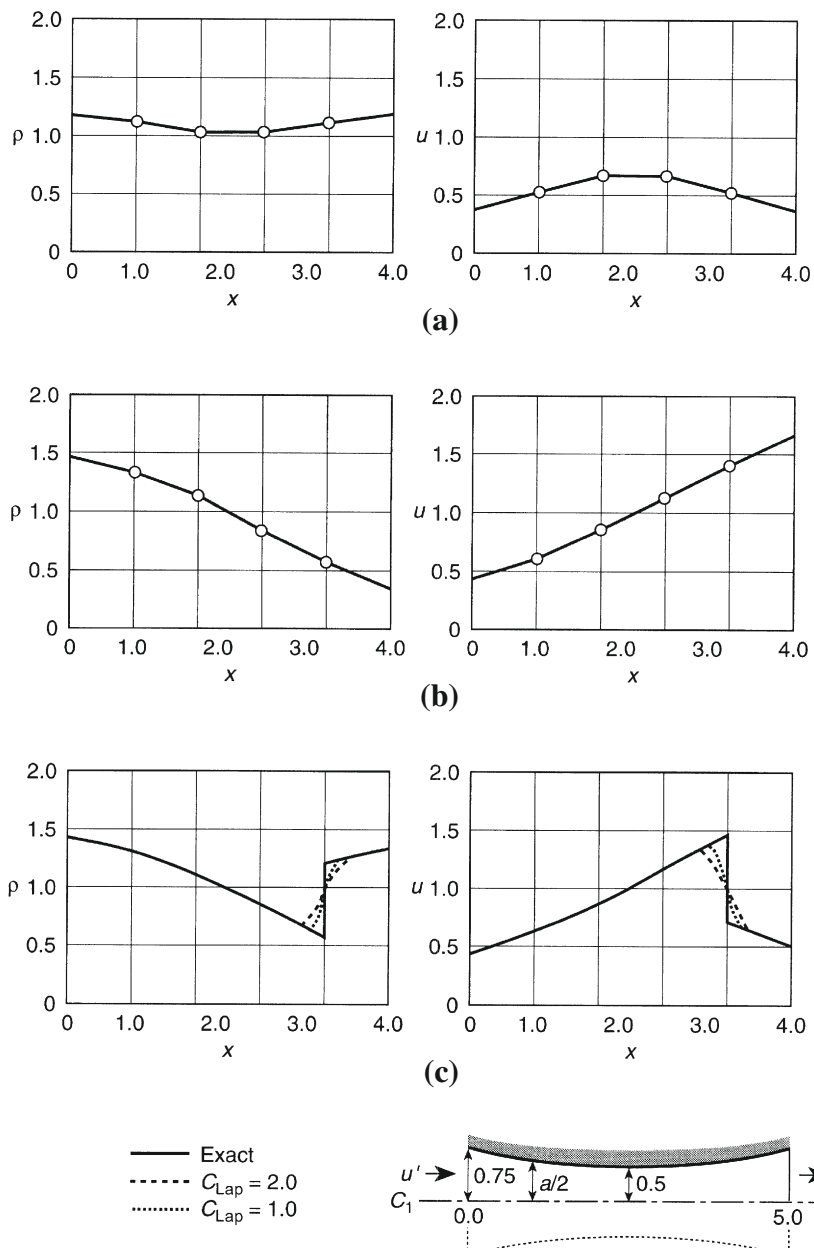
The Riemann shock tube problem [1, 69]. The total length is divided into 100 elements. Profile illustrated corresponds to 70 time steps ($\Delta t = 0.25$). Lapidus constant $C_{\text{Lap}} = 1.0$.

Example 7.2. Isothermal flow through a nozzle in one dimension

Here a variant of the Euler equation is used in which isothermal conditions are assumed and in which the density is replaced by ρa where a is the cross-sectional area [1] assumed to vary as [70]

$$a = 1.0 + \frac{(x - 2.5)^2}{12.5} \quad \text{for } 0 \leq x \leq 5 \quad (7.21)$$

The speed of sound is constant as the flow is isothermal and various conditions at inflow and outflow limits were imposed as shown in Fig. 7.6. In all problems steady

**FIGURE 7.6**

Isothermal flow through a nozzle [1]. Forty elements of equal size used: (a) subsonic inflow and outflow; (b) supersonic inflow and outflow; (c) supersonic inflow–subsonic outflow with shock.

state was reached after some 500 time steps. For the case with supersonic inflow and subsonic outflow, a shock forms and Lapidus-type artificial diffusion was used to deal with it, showing in Fig. 7.6c the increasing amount of “smearing” as the coefficient C_{Lap} is increased.

Example 7.3. Two-dimensional transient supersonic flow over a step

This final example concerns the transient initiation of supersonic flow in a wind tunnel containing a step. The problem was first studied by Woodward and Colella [71] and the results of Ref. [5] presented here are essentially similar.

In this problem a uniform mesh of linear triangles, shown in Fig. 7.7, was used and no difficulties of computation were encountered although a Lapidus constant $C_{\text{Lap}} = 2.0$ had to be used due to the presence of shocks.

Example 7.4. Inviscid flow past a NACA0012 aerofoil

This is one of the widely studied problems in aerodynamics that has a large number of benchmark steady-state data. Here we have solved this problem over a range of Mach numbers within subsonic, transonic, and supersonic flow regimes at zero angle of attack. The problem domain and mesh used are shown in Figure 7.8. The diameter of the circular domain is equal to 25 times the chord length of the aerofoil. The leading edge of the aerofoil is assumed to be at the center of the domain. All the inlet quantities are prescribed and no variable is prescribed at the exit at supersonic and transonic speeds. At subsonic speeds however, one of the primitive variables is prescribed at the exit. The Mach number is varied between 0.25 and 1.2 to capture all different flow regimes.

Figure 7.9 shows the steady-state convergence histories at different Mach numbers. As expected convergence to steady state at supersonic and transonic Mach numbers is rapid but the subsonic cases took longer to reach steady state. The pressure coefficients are calculated as $-2(p_a - p_{\text{ref}})$. Here p_{ref} is the reference pressure at inlet.

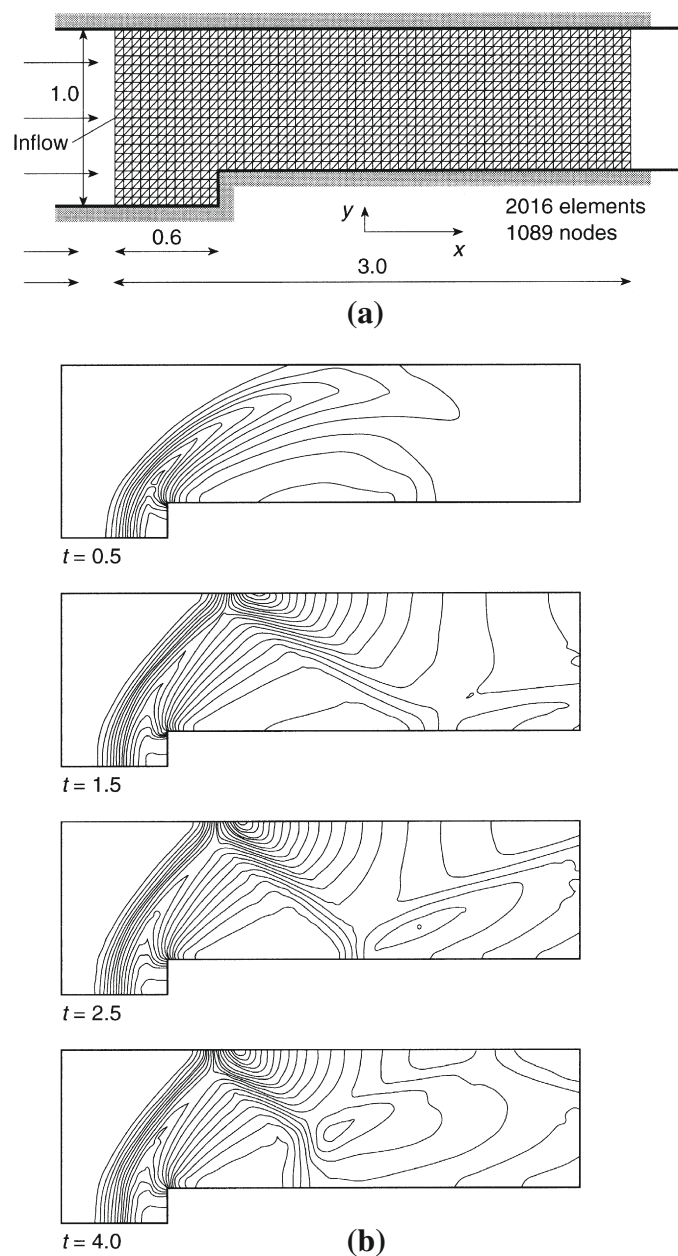
Figures 7.10 and 7.11 show the pressure contours and surface pressure coefficient distribution at subsonic Mach numbers. At both subsonic Mach numbers, we invoke the variable smoothing in the place of shock capturing viscosities. A detailed comparison of stagnation quantities with an analytical solution at subsonic Mach numbers is presented in Ref. [68].

Figures 7.12 and 7.13 show the pressure contours and surface pressure coefficient distribution at transonic and supersonic Mach numbers. In Figure 7.13 pressure coefficient results at two Mach numbers are compared with the AGARD results [72].

7.8 Adaptive refinement and shock capture in Euler problems

7.8.1 General

The examples of the previous section have indicated the formation of shocks both in transient and steady-state problems of high-speed flow. Clearly the resolution of

**FIGURE 7.7**

Transient supersonic flow over a step in a wind tunnel [5] (problem of Woodward and Colella [71]). Inflow Mach 3 uniform flow: (a) structured uniform mesh; (b) solution – contours of pressure at various times.

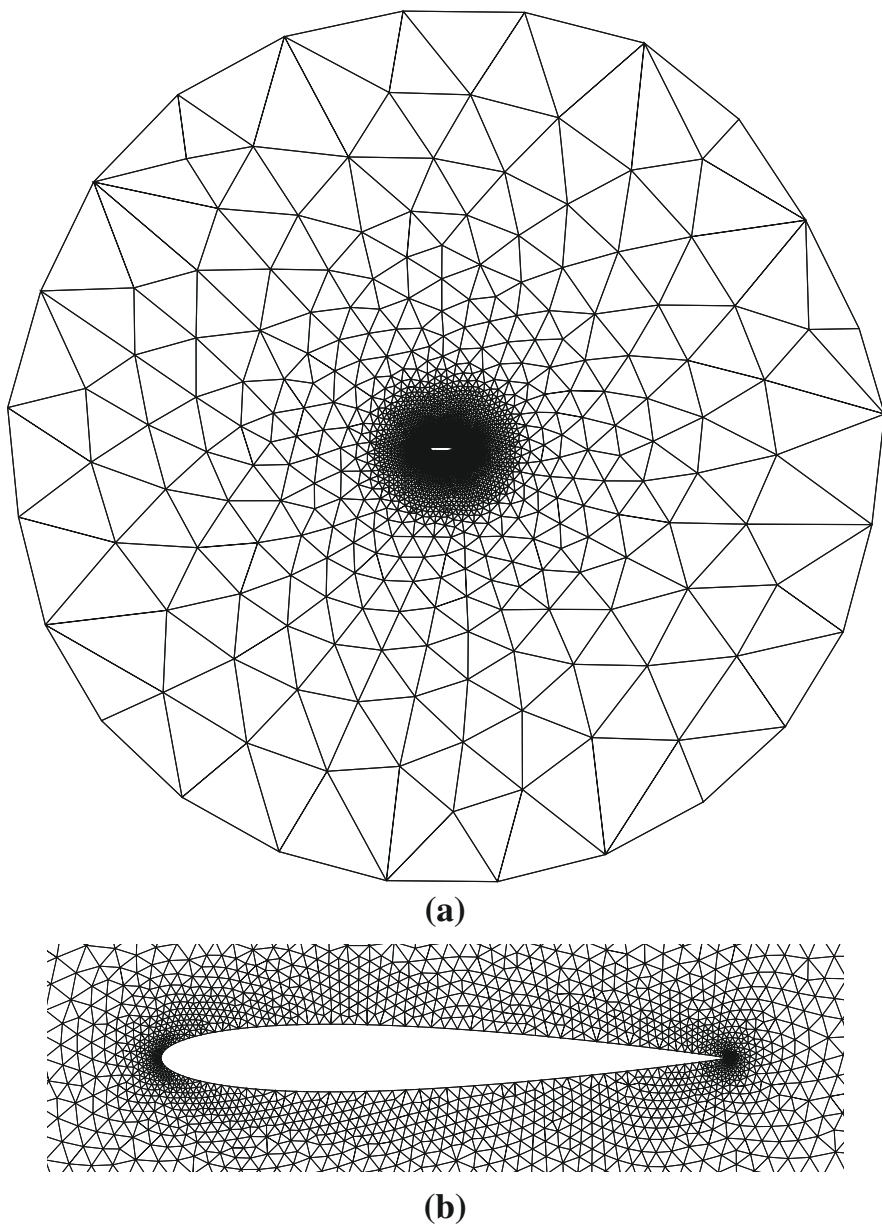
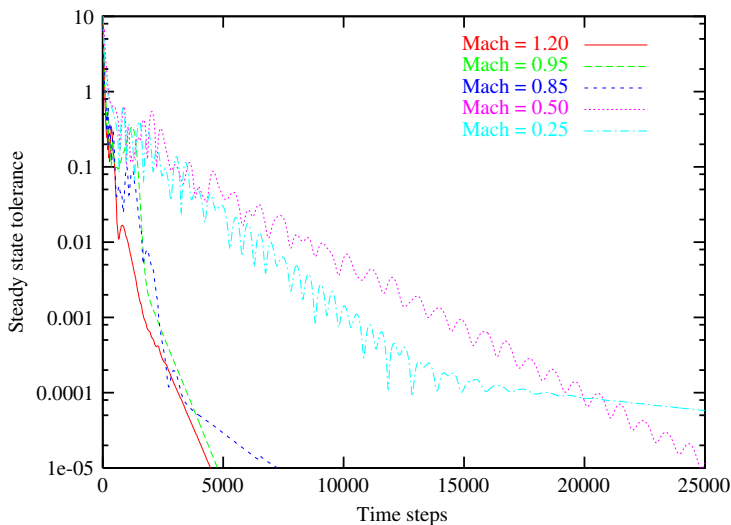
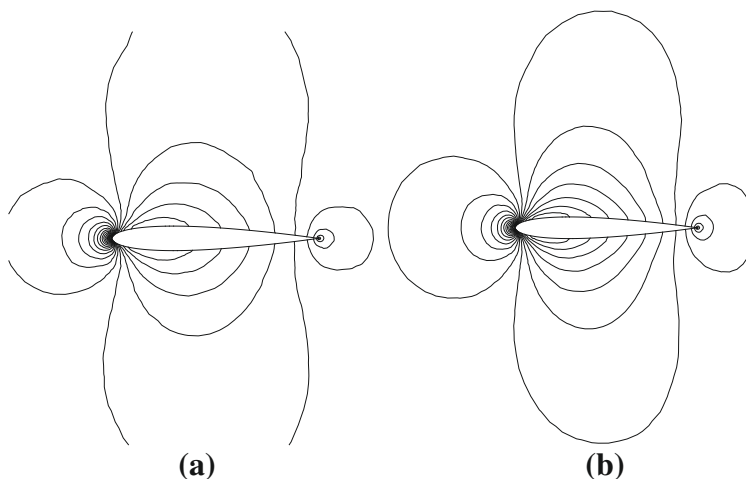


FIGURE 7.8

Inviscid flow past a NACA0012 aerofoil. Unstructured mesh. Number of nodes: 3753; number of elements: 7351. (a) Finite element mesh and domain; (b) mesh distribution in the vicinity of the aerofoil.

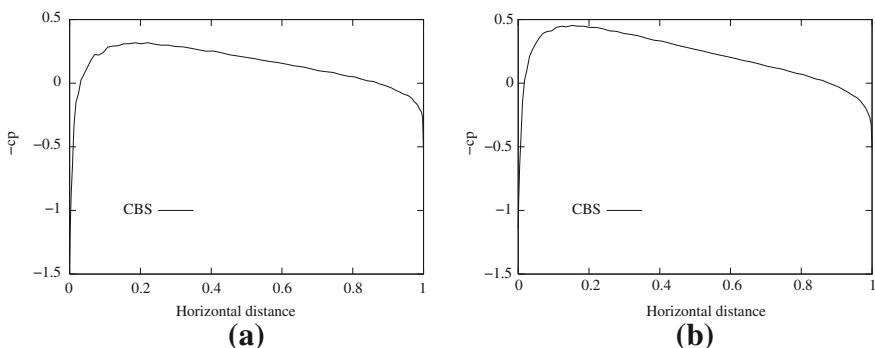
**FIGURE 7.9**

Inviscid flow past a NACA0012 aerofoil. Convergence histories to steady state.

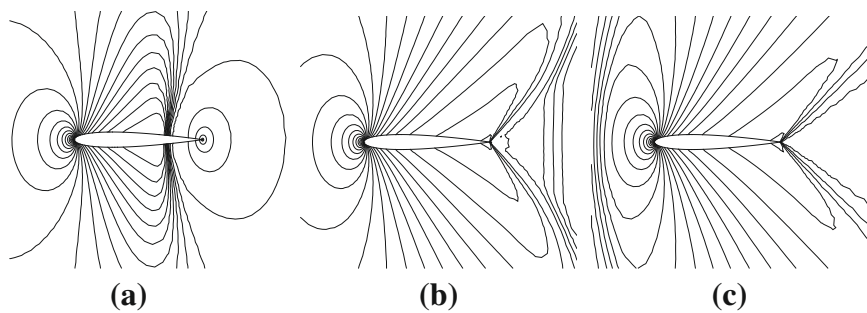
**FIGURE 7.10**

Inviscid subsonic flow past a NACA0012 aerofoil. Pressure contours: (a) Mach number = 0.25; (b) Mach number = 0.5.

such discontinuities or near discontinuities requires a very fine mesh. Here the use of “engineering judgement,” which is often used in solid mechanics by designing *a priori* mesh refining near singularities posed by corners in the boundary, etc., can no

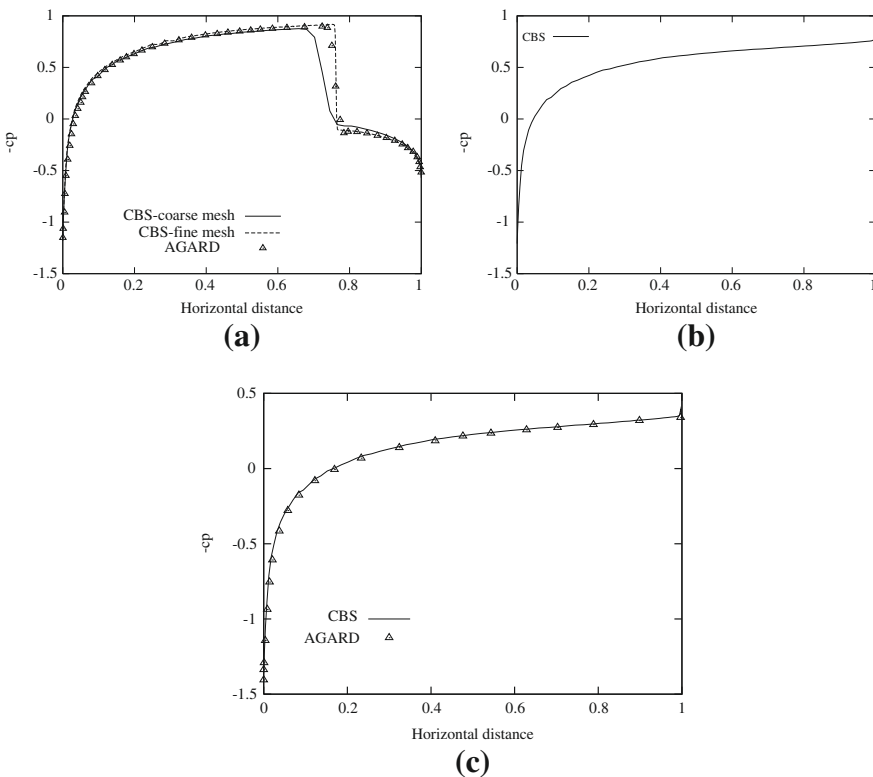
**FIGURE 7.11**

Inviscid subsonic flow past a NACA0012 aerofoil. Pressure coefficient distribution:
(a) Mach number = 0.25; (b) Mach number = 0.5.

**FIGURE 7.12**

Inviscid transonic and supersonic flow past a NACA0012 aerofoil. Pressure contours:
(a) Mach number = 0.85; (b) Mach number = 0.95; (c) Mach number = 1.2.

longer be used. In problems of compressible flow the position of shocks, where the refinement is most needed, is not known in advance. For this and other reasons, the use of adaptive mesh refinement based on error indicators is essential for obtaining good accuracy and “capturing” the location of shocks. It is therefore not surprising that the science of adaptive refinement has progressed rapidly in this area and indeed, as we shall see later, has been extended to deal with Navier-Stokes equations where a higher degree of refinement is also required in boundary layers. We have discussed the history of such adaptive development and procedures for its use in [Section 4.3](#), [Chapter 4](#).

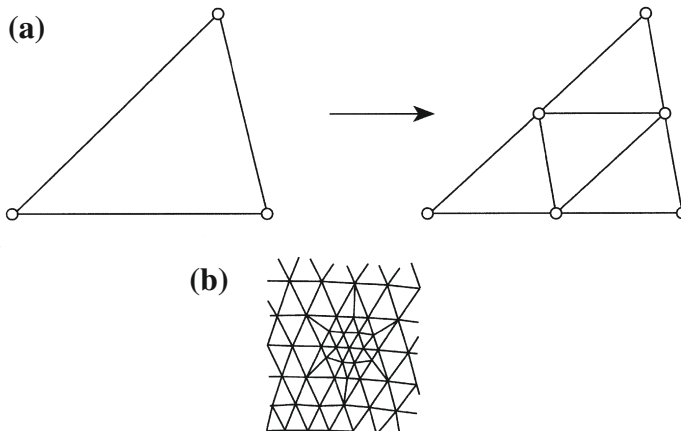
**FIGURE 7.13**

Inviscid transonic and supersonic flow past a NACA0012 aerofoil. Pressure coefficient distribution: (a) Mach number = 0.85; (b) Mach number = 0.95; (c) Mach number = 1.2.

7.8.2 The *h*-refinement process and mesh enrichment

Once an approximate solution has been achieved on a given mesh, the local errors can be evaluated and new element sizes (and elongation directions if used) can be determined for each element. For some purposes it is again convenient to transfer such values to the nodes so that they can be interpolated continuously. The procedure here is of course identical to that of smoothing the derivatives discussed in [Section 4.3, Chapter 4](#).

To achieve the desired accuracy various procedures can be used. The most obvious is the process of *mesh enrichment* in which the existing mesh is locally subdivided into smaller elements still retaining the “old” mesh in the configuration. [Figure 7.14a](#) shows how triangles can be readily subdivided in this way. With such enrichment an obvious connectivity difficulty appears. This concerns the manner in which the subdivided elements are connected to ones not so refined. A simple process is illustrated showing

**FIGURE 7.14**

Mesh enrichment. (a) Triangle subdivision. (b) Restoration of connectivity.

element halving in the manner of Fig. 7.14b. Here of course it is fairly obvious that this process, first described in Ref. [73], can only be applied in a gradual manner to achieve the predicted subdivisions. However, element elongation is not possible with such mesh enrichment.

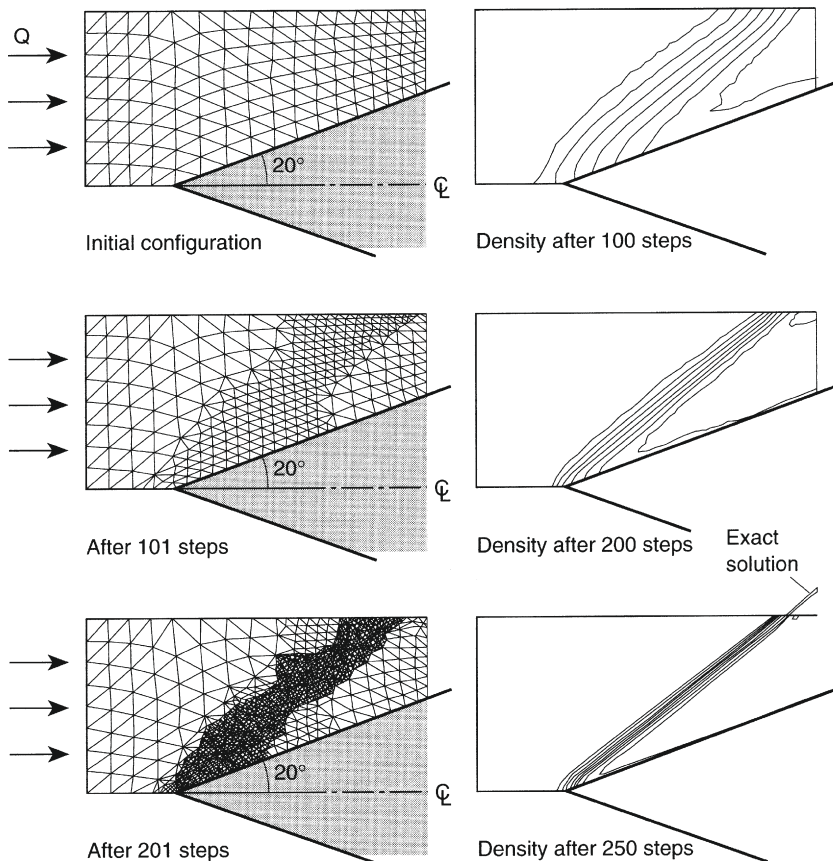
Despite such drawbacks the procedure is very effective in localizing (or capturing) shocks, as we illustrate in Fig. 7.15.

In Fig. 7.15, the theoretical solution is simply one of a line discontinuity shock in which a jump of all the components of Φ occurs. The original analysis carried out on a fairly uniform mesh shows a very considerable “blurring” of the shock. In Fig. 7.15 we also show the refinement being carried out at two stages and we see how the shock is progressively reduced in width.

In the above example, the mesh enrichment preserved the original, nearly equilateral, element form with no elongation possible.

Whenever a sharp discontinuity is present, local refinement will proceed indefinitely as curvatures increase without limit. Precisely the same difficulty indeed arises in mesh refinement near singularities for elliptic problems [74] if local refinement is the only guide. In such problems, however, the limits are generally set by the overall energy norm error consideration and the refinement ceases automatically. In the present case, the limit of refinement needs to be set and we generally achieve this limit by specifying the *smallest element size* in the mesh.

The *h*-refinement of the type proposed can of course be applied in a similar manner to quadrilaterals. Here clever use of data storage allows the necessary refinement to be achieved in a few steps by ensuring proper transitions [75].

**FIGURE 7.15**

Supersonic, Mach 3, flow past a wedge. Exact solution forms a stationary shock. Successive mesh enrichment and density contours.

7.8.3 *h*-refinement and remeshing in steady-state two-dimensional problems

Many difficulties mentioned above can be resolved by *automatic generation of meshes of a specified density*. Such automatic generation has been the subject of much research in many applications of finite element analysis. We have discussed this subject in [Section 4.3, Chapter 4](#). The closest achievement of a prescribed element size and directionality can be obtained for triangles and tetrahedra. Here the procedures developed by Peraire et al. [11, 14] are most direct and efficient, allowing element stretching in prescribed directions (though of course the amount of such stretching is sometimes restricted by practical considerations).

We refer the reader for details of such mesh generation to the original publications. In the examples that follow we shall exclusively use this type of mesh adaptivity.

Example 7.5. Inviscid flow with shock reflection from a solid wall

In Fig. 7.16 we show a simple example [11] of shock wave reflection from a solid wall. Here only a typical “cutout” is analyzed with appropriate inlet and outlet conditions imposed. The elongation of the mesh along the discontinuity is clearly shown. The solution was remeshed after the iterations nearly reached a steady state.

Example 7.6. Hypersonic inviscid flow past a blunt body

In Fig. 7.17 a somewhat more complex example of *hypersonic flow* around a blunt, two-dimensional obstacle is shown. Here it is of interest to note that:

1. A detached shock forms in front of the body.
2. A very coarse mesh suffices in front of such a shock where simple free stream flow continues and the mesh is made “finite” by a maximum element size prescription.
3. For the same minimum element size a reduction of degrees of freedom is achieved by refinement which shows much improved accuracy.

For such hypersonic problems, it is often claimed that special methodologies of solution need to be used. References [24, 76, 26] present quite sophisticated methods for dealing with such high-speed flows.

Example 7.7. Supersonic inviscid flow past a full circular cylinder

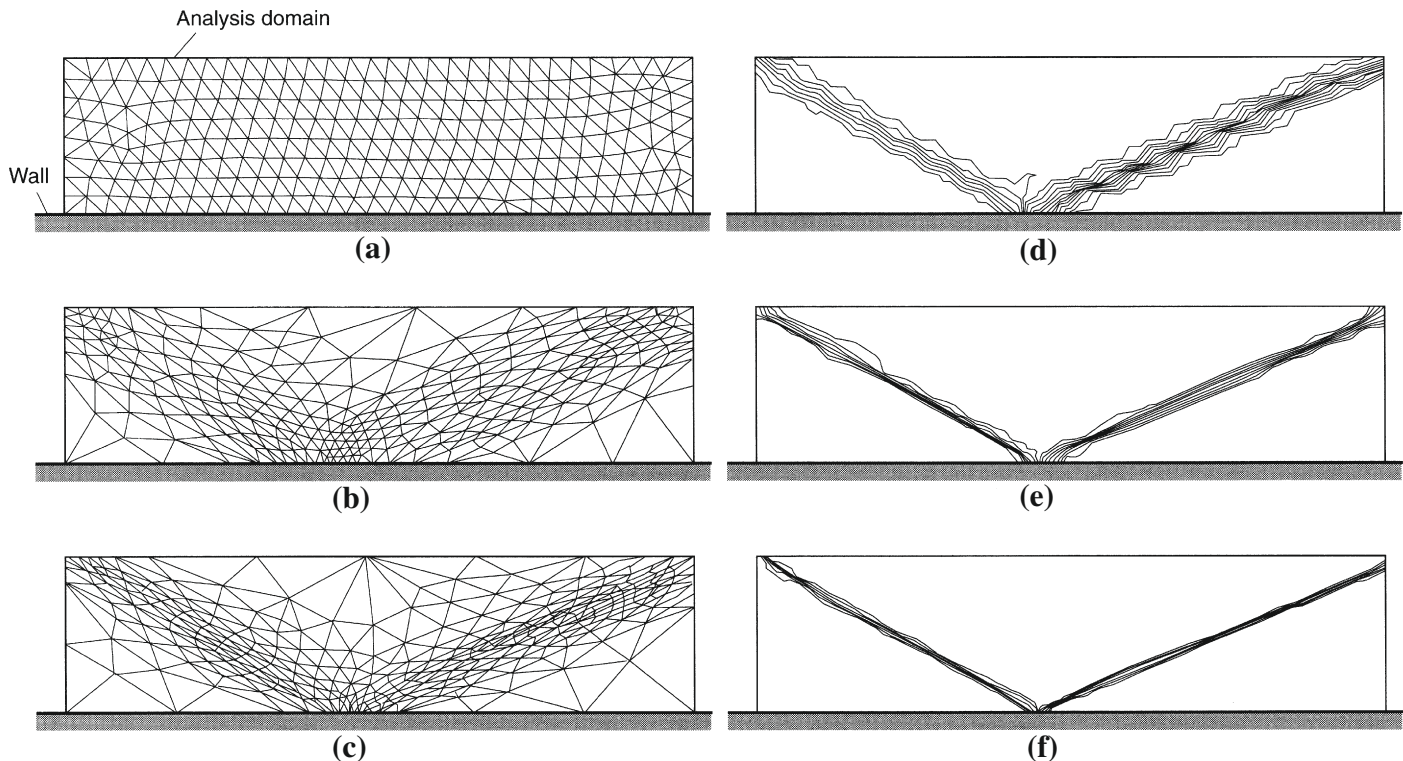
In Figs. 7.18 and 7.19, we show the results of supersonic Mach 3 flow past a full cylinder [61]. The mesh (Fig. 7.18b) is adapted along the shock front to get a good resolution of the shock. The mesh behind the cylinder is very fine to capture the complex motion. In Figs. 7.18c and d, the Mach contours are obtained using the CBS algorithm using the second derivative-based shock capture and residual-based shock capture respectively. In Fig. 7.19, the coefficient of pressure values and Mach number distribution along the mid-height through the surface of the cylinder are presented. Here the results generated by the MUSCL [24] scheme are also plotted for the sake of comparison.

Example 7.8. Inviscid shock interaction

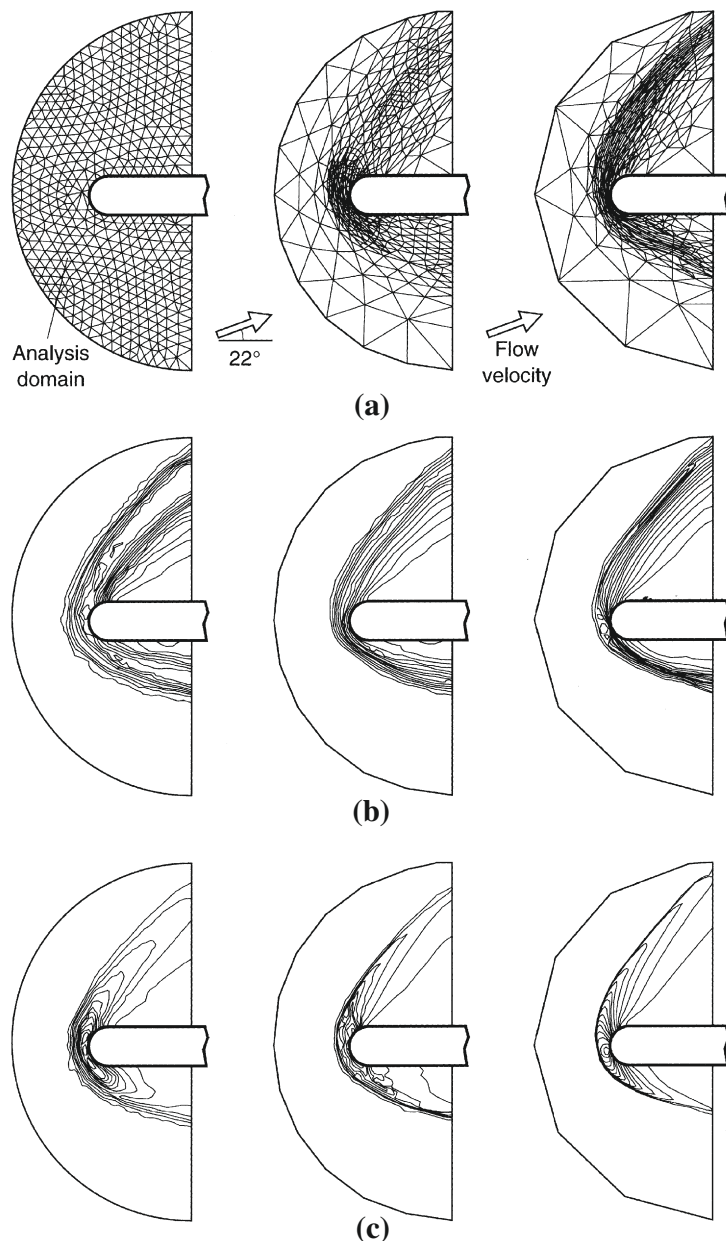
Figure 7.20 shows a yet more sophisticated example in which an impinging shock interacts with a bow shock [77].

7.9 Three-dimensional inviscid examples in steady state

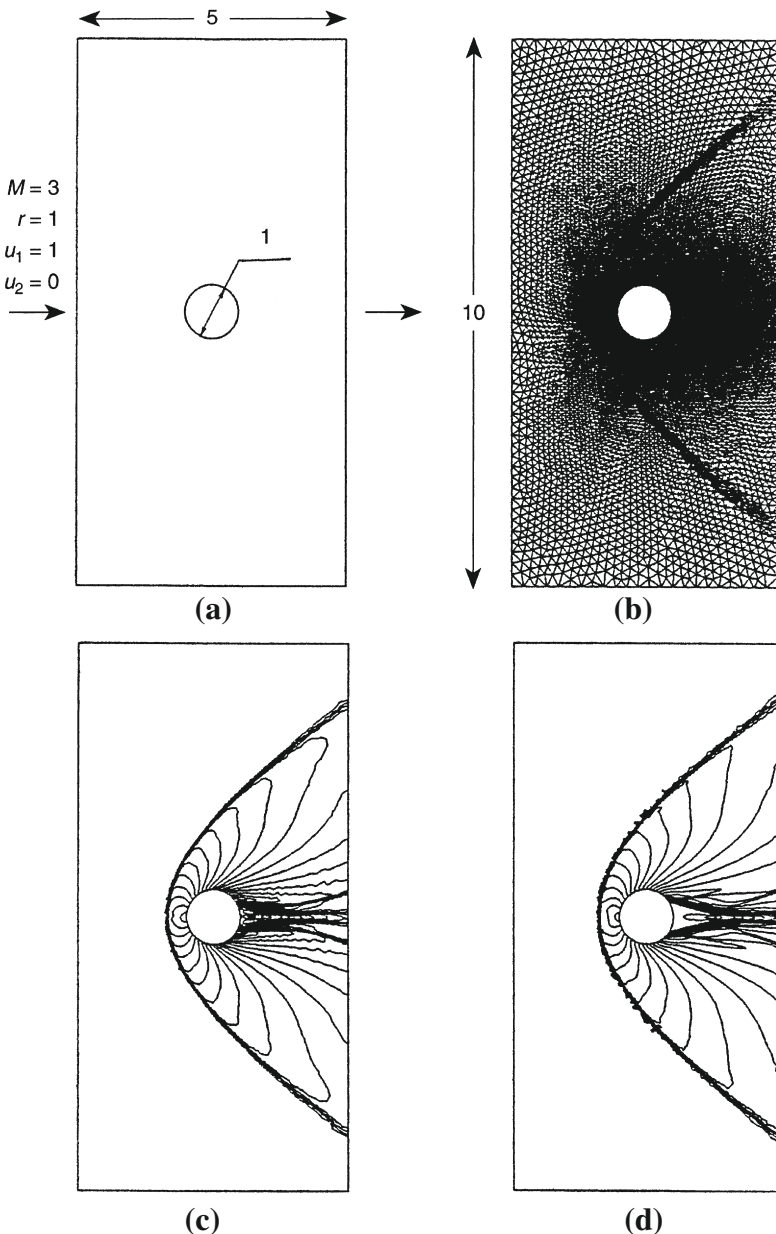
Two-dimensional problems in fluid mechanics are much rarer than two-dimensional problems in solid mechanics and invariably they represent a very crude approximation to reality. Even the problem of an aerofoil cross-section, which we have discussed previously, hardly exists as a two-dimensional problem as it applies only to infinitely long wings. For this reason attention has largely been focused, and much creative

**FIGURE 7.16**

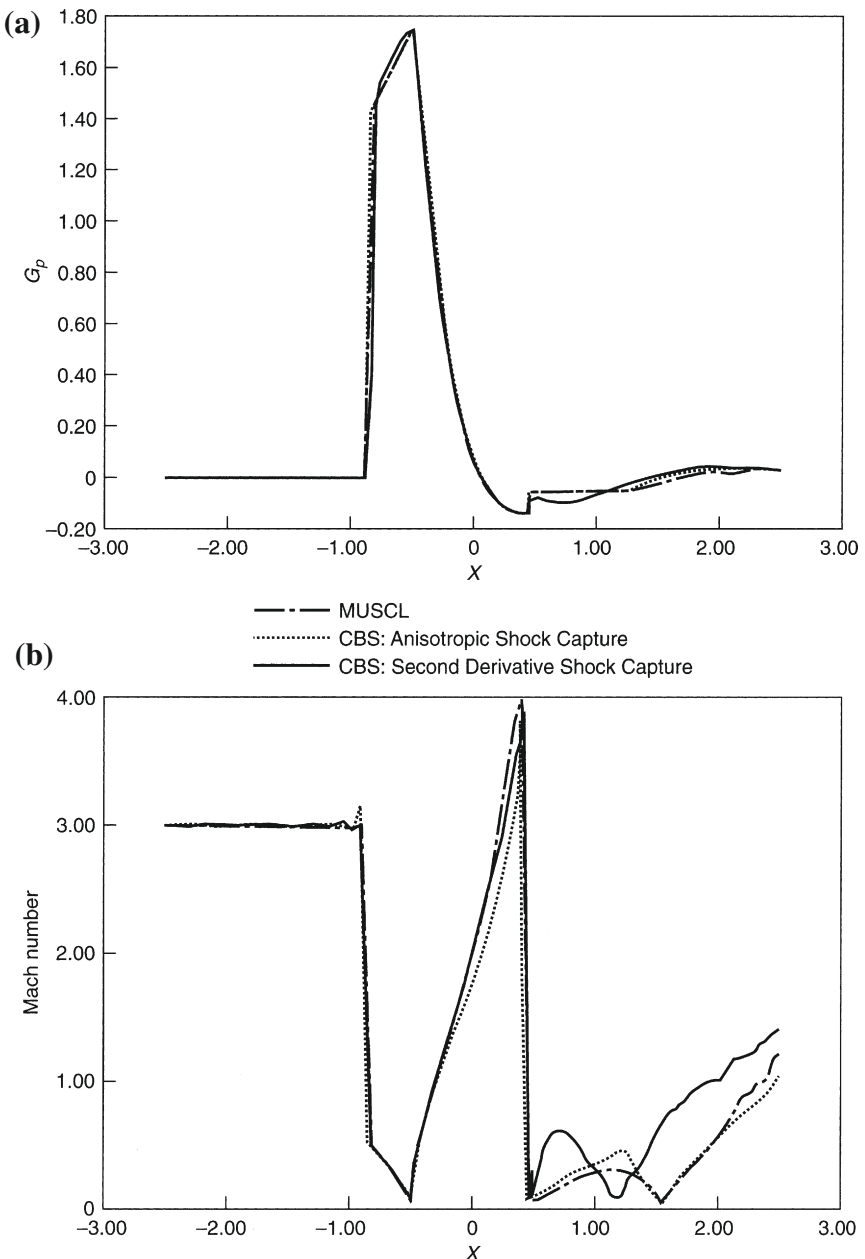
Reflection of a shock wave at a wall [11]: Euler equations. A sequence of meshes: (a) nodes: 279, elements: 478; (b) nodes: 265, elements: 479; (c) nodes: 285, elements: 528; and corresponding pressure contours, (d) to (f).

**FIGURE 7.17**

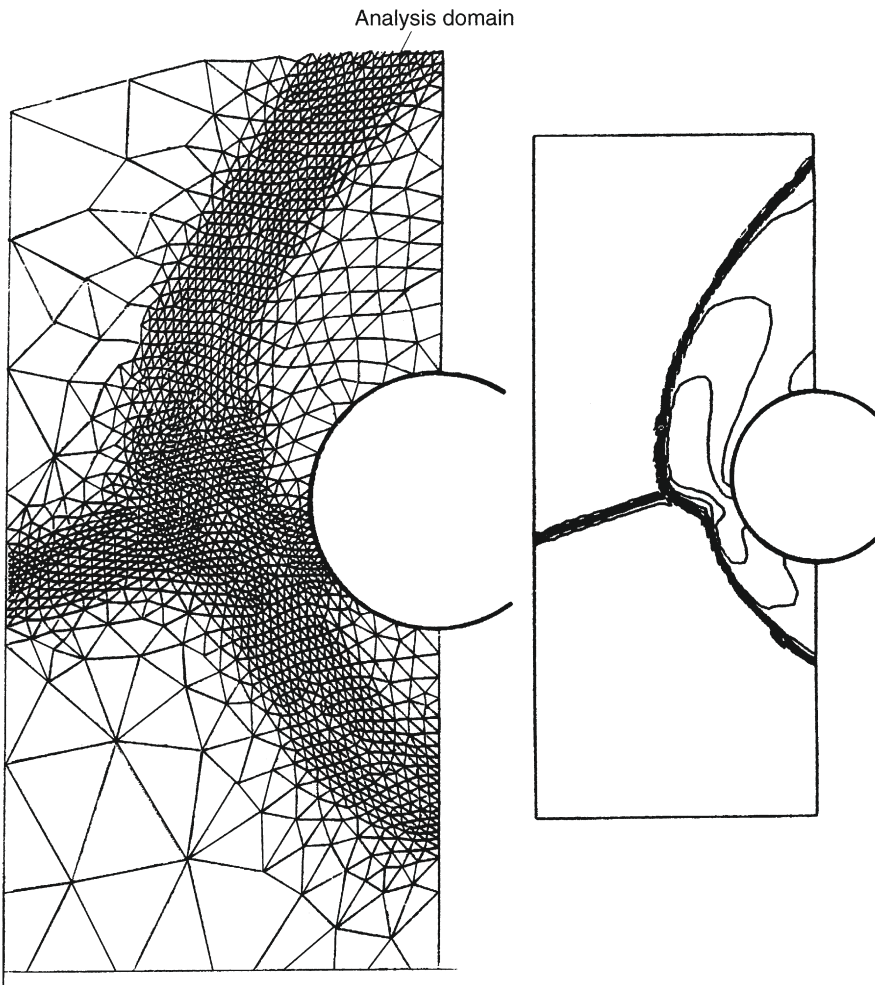
Hypersonic flow past a blunt body [11] at Mach 25, 22° angle of attack. (a) Sequence of meshes deployed; (b) the corresponding density; (c) the corresponding pressure contours. Initial mesh, nodes: 547, elements: 978; first mesh, nodes: 383, elements: 696; final mesh, nodes: 821, elements: 1574.

**FIGURE 7.18**

Supersonic flow past a full cylinder [61]. $M = 3$: (a) geometry and boundary conditions; (b) adapted mesh, nodes: 12651, elements: 24,979; (c) Mach contours using second derivative shock capture; (d) Mach contours using anisotropic shock capture.

**FIGURE 7.19**

Supersonic flow past a full cylinder [61]. $M = 3$: comparison of (a) coefficient of pressure, (b) Mach number distribution along the mid-height and cylinder surface.

**FIGURE 7.20**

Interaction of an impinging and bow shock wave [77]. Adapted mesh and pressure contours.

research done, in developing three-dimensional codes for solving realistic problems. In this section we shall consider some examples derived by the use of such three-dimensional codes and in all these the basic element used will be the tetrahedron, which now replaces the triangle of two dimensions. Although the solution procedure and indeed the whole formulation in three dimensions is almost identical to that described for two dimensions, it is clear that the number of unknowns will increase very rapidly when realistic problems are dealt with. It is common when using linear

elements to encounter several million variables as unknowns and for this reason here, more than anywhere else, iterative processes are necessary.

Indeed much effort has gone into the development of special procedures of solution which will accelerate the iterative convergence and which will reduce the total computational time. In this context we should mention three approaches which are of help.

The recasting of element formulation in an edge form

Here a considerable reduction of storage can be achieved by this procedure and some economies in computational time achieved. We have not discussed this matter in detail but refer the reader to Ref. [30] where the method is fully described and for completeness we summarize the essential features of edge formulation in [Appendix F](#).

Multigrid approaches

In the standard iteration we proceed in a time frame by calculating point by point the changes in various quantities and we do this on the finest mesh. As we have seen this may become very fine if adaptivity is used locally. In the multigrid solution, as initially introduced into the finite element field, the solution starts on a coarse mesh, the results of which are used subsequently for generating the first approximation to the fine mesh. Several iterative steps are then carried out on the fine mesh. In general a return to the coarse mesh is then made to calculate the changes of residuals there and the process is repeated on several meshes done subsequently. This procedure can be used on several meshes and the iterative process is much accelerated. We discuss this process in [Appendix H](#) in a little more detail. However, we quote here several references [78–83] in which such multigrid procedures have been used and these are of considerable value.

Multigrid methods are obviously designed for meshes which are “nested,” i.e., in which coarser and finer mesh nodes coincide. This need not be the case generally. In many applications completely different meshes of varying density are used at various stages.

Parallel computation

The third procedure for reducing the solution time is to use parallelization. We do not discuss it here in detail as the matter is potentially coupled with the computational aspects of the problem. Here the reader should consult the current literature on the subject [31,37].

In what follows we shall illustrate three-dimensional applications on a few inviscid examples as this section deals with Euler problems. However in [Section 7.12](#) we shall return to a formulation using viscous Navier-Stokes equations.

7.9.1 Solution of the flow pattern around a complete aircraft

In the early days of numerical analysis applied to computational fluid dynamics which used finite differences, no complete aircraft was analyzed as in general only structured meshes were admissible. The analysis thus had to be carried out on isolated components of the aircraft as shown in [Figure 7.21](#). Later construction of distorted and partly structured meshes increased the possibility of analysis. Nevertheless the first complete aircraft analyses were done only in the mid-1980s. In all of these, finite elements using unstructured meshes were used (though we include here the finite volume formulation which was almost identical to finite elements and was used by Jameson et al. [85]). The very first aircraft was the one dealt with using potential theory in the Dassault establishment. The results were published later by Periaux and coworkers [86]. Very shortly after that a complete supersonic aircraft was analyzed by Peraire et al. [84] in Swansea in 1987.

Example 7.9. Inviscid flow past full aircraft

[Figure 7.22](#) shows the aircraft analyzed in Swansea [84], which is a supersonic fighter of generic type at Mach 2. The analysis was made slightly adaptive though adaptivity was not carried very far (due to cost). Nevertheless the refinement localized the shocks which formed.

In the analysis some 125,000 elements were used with approximately 70,000 nodes and therefore some 350,000 variables. This of course is not a precise analysis and many more variables would be used currently to get a more accurate representation of flow and pressure variables.

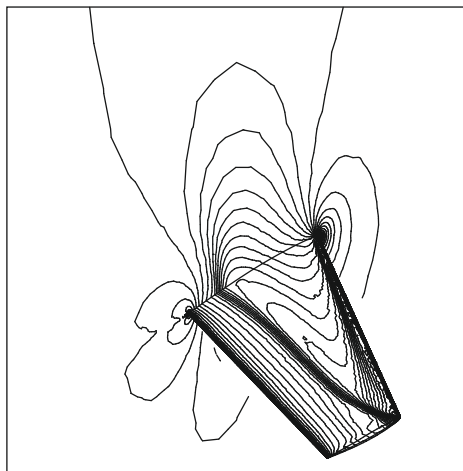
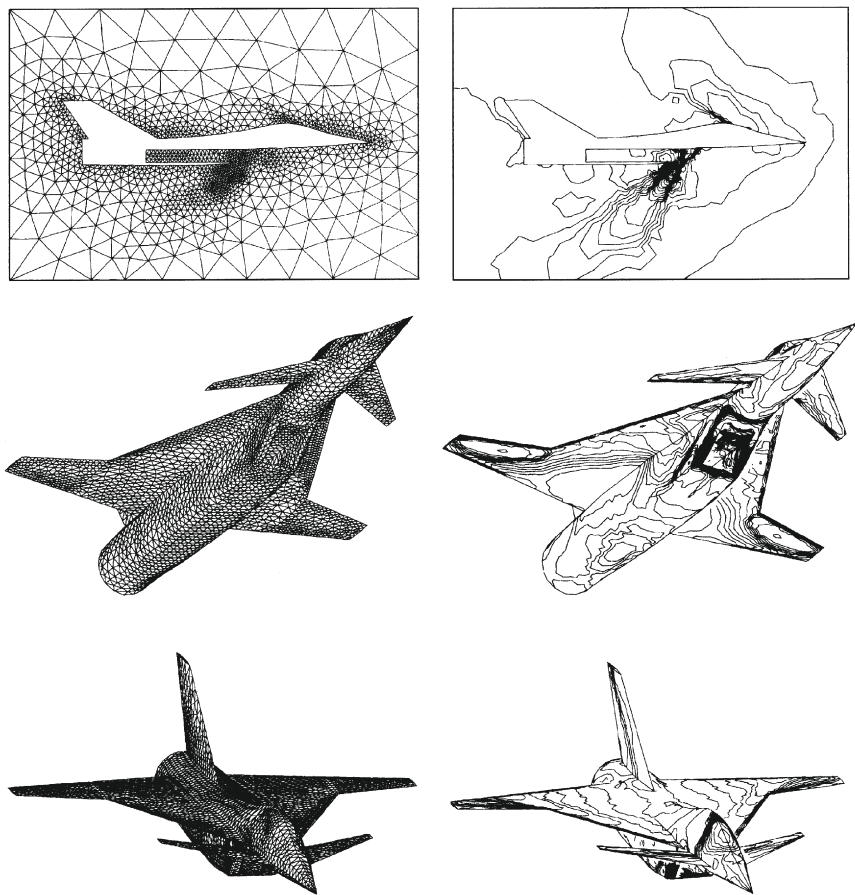


FIGURE 7.21

Inviscid flow past an ONERA M6 wing. Density contours. Mach number = 0.78, angle of attack to horizontal = 2.8° .

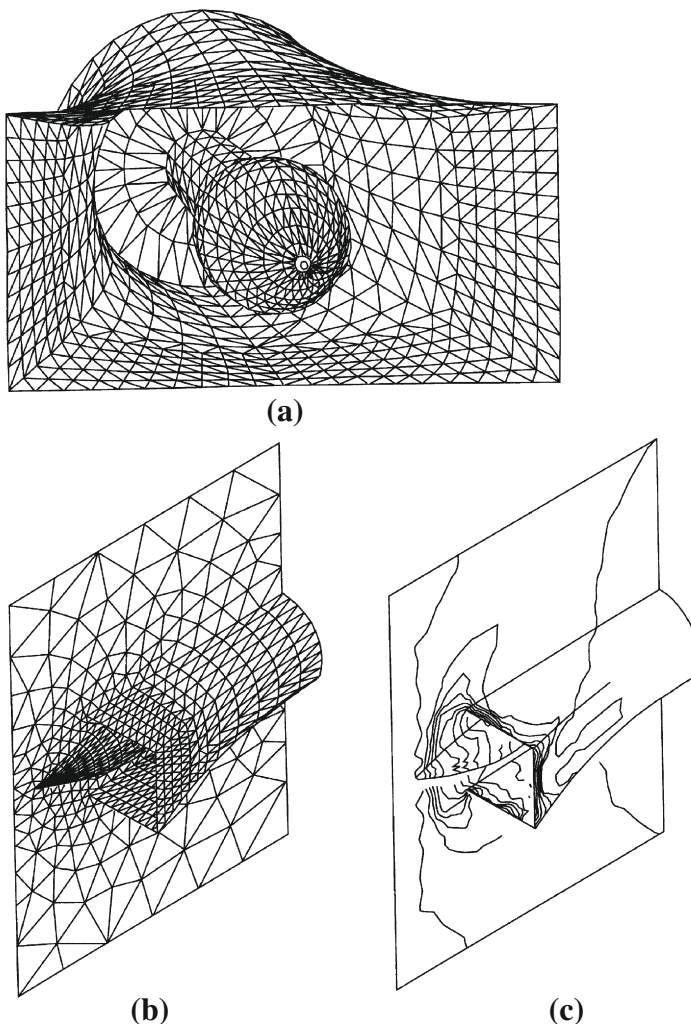
**FIGURE 7.22**

Adaptive three-dimensional solution of compressible inviscid flow around a high-speed (Mach 2) aircraft [84]. Nodes: 70,000, elements: 125,000.

A more sophisticated analysis is given in Ref. [26]. Here a civil aircraft in subsonic flow is modeled and this illustrates the use of multigrid methods. In this particular multigrid applications three meshes of different refinement were used and the iteration is fully described in Ref. [26]. In this example the total number of unknown quantities was 1,616,000 in the finest mesh.

Example 7.10. Inviscid engine intake

There are many other three-dimensional examples which could at this stage be quoted but we only show here a three-dimensional analysis of an engine intake [84] at Mach 2. This is given in Fig. 7.23.

**FIGURE 7.23**

Three-dimensional analysis of an engine intake [84] at Mach 2 (14,000 elements): (a) mesh on analysis surface; (b) mesh on analysis surface; (c) pressure contours.

7.9.2 THRUST: The supersonic car

A very similar problem to that posed by the analysis of the whole aircraft was given by the team led by Professor Morgan. This was the analysis of a car which was attempting to create the world speed record by establishing this in the supersonic range [35,36,87]. This attempt was indeed successfully made on October 15, 1997.

Unlike in the problem of the aircraft, the alternative of wind tunnel tests was not available. While in aircraft design, wind tunnels which are supersonic and subsonic

are well used in practice (though at a cost which is considerably more than that of a numerical analysis) the possibility of doing such a test on a motor car was virtually nonexistent. The reason for this is the fact that the speed of the air flow past the body of the car and the speed of the ground relative to the car are identical. Any test would therefore require the bed of the wind tunnel to move at a speed in excess of 750+ miles an hour. For this reason calculations were therefore preferable.

The moving ground will of course create a very important boundary layer such as that which we will discuss in later sections. However the simple omission of viscosity permitted the inviscid solution by a standard Euler-type program to be used. It is well known that the Euler solution is perfectly capable of simulating all shocks very adequately and indeed results in very well-defined pressure distributions over the bodies whether it is over an aircraft or a car. The object of the analysis was indeed that of determining such pressure distributions and the lift caused by these pressures. It was essential that the car should remain on the ground, indeed this is one of the conditions of the ground speed record and any design which would result in substantial lift overcoming the gravity on the car would be disastrous for obvious reasons.

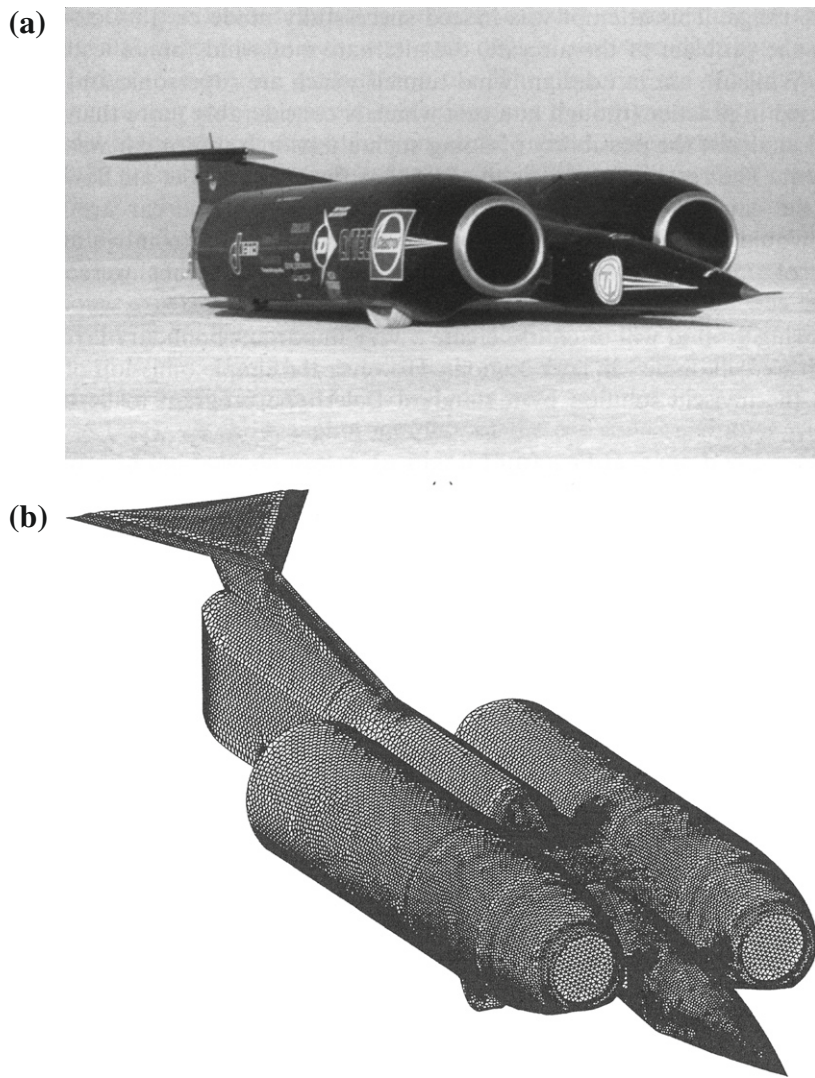
The complete design of the supersonic car was thus made with several alternative geometries until the computer results were satisfactory. Here it is interesting however to have some experimental data and the preliminary configuration was tested by a rocket driven sled. This was available for testing rocket projectiles at Pendine Sands, South Wales, UK. Here a 1:25 scale model of the car was attached to such a rocket and 13 supersonic and transonic runs were undertaken.

In Fig. 7.24a, we show a photograph [35] of the car concerned after winning the speed record in the Nevada desert. In Fig. 7.24b a surface mesh is presented from which the full three-dimensional mesh at the surrounding atmosphere was generated (surface mesh, nodes: 39,528, elements: 79,060; volume mesh, nodes: 134,272, elements: 887,634).

In Fig. 7.25, pressure contours [35] on the surface of the car body are given. In Fig. 7.26, a detailed comparison of CFD results [35] with experiments is shown. The results of this analysis show a remarkable correlation with experiments. The data points which do not appear close to the straight line are the result of the sampling point being close to, but the wrong side of, a shock wave. If conventional correlation techniques for inviscid flow (viscous correction) are applied, these data points also lie on the straight line. In total, nine pressure points were used situated on the upper and lower surfaces of the car. The plot shows the comparison of pressures at specific positions on the car for Mach numbers of 0.71, 0.96, 1.05, and 1.08.

7.10 Transient two- and three-dimensional problems

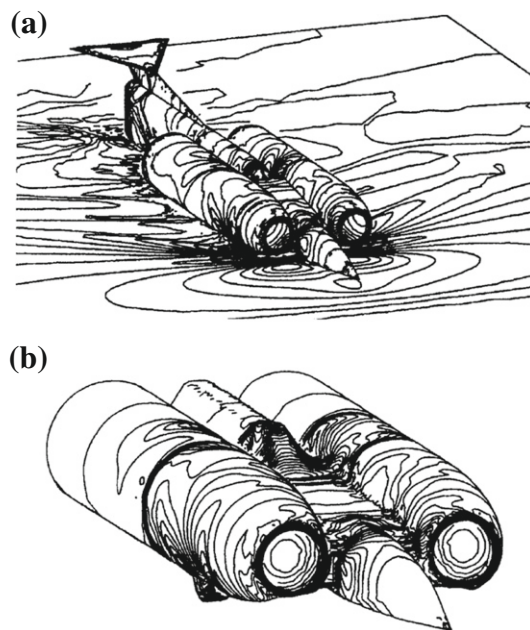
In all of the previous problems the time stepping was used simply as an iterative device for reaching the steady-state solutions. However this can be used in real time and the transient situation can be studied effectively. Many such transient problems have been dealt with from time to time and here we illustrate the process on three examples.

**FIGURE 7.24**

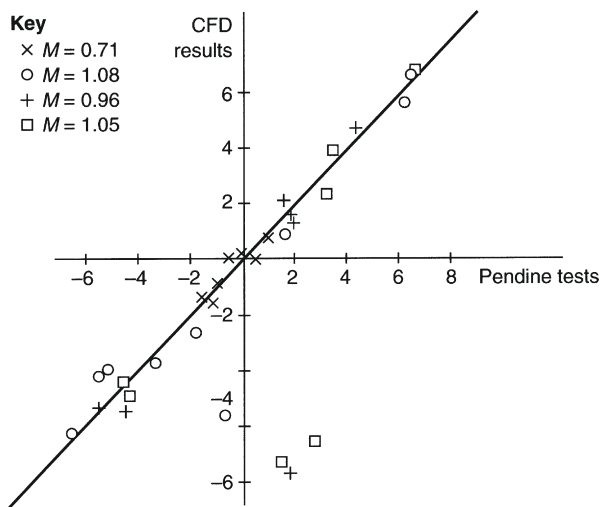
Supersonic car, THRUST SSC [35]. (a) Car and (b) finite element surface mesh. (*Image used in (a) courtesy of SSC Programme Ltd. Photographer Jeremy C.R. Davey.*)

Example 7.11. Exploding pressure vessel

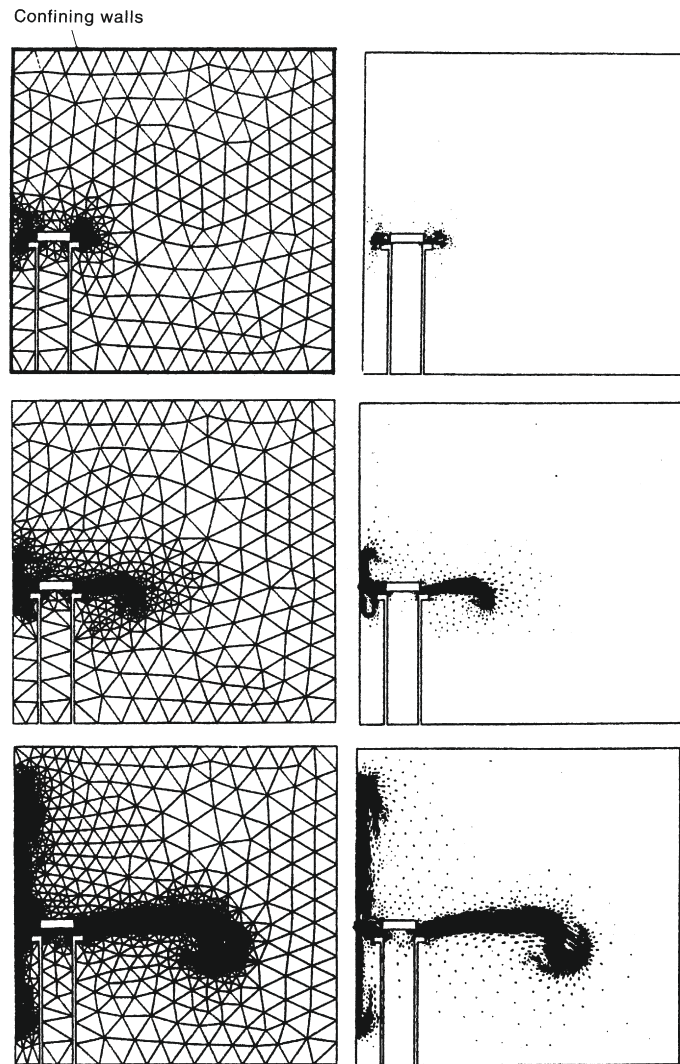
The first one concerns an exploding pressure vessel [71] as a two-dimensional model as shown in Fig. 7.27. Here of course adaptivity had to be used and the mesh is regenerated every few steps to reproduce the transient motion of the shock front.

**FIGURE 7.25**

Supersonic car, THRUST SSC [35] pressure contours: (a) full configuration; (b) front portion.

**FIGURE 7.26**

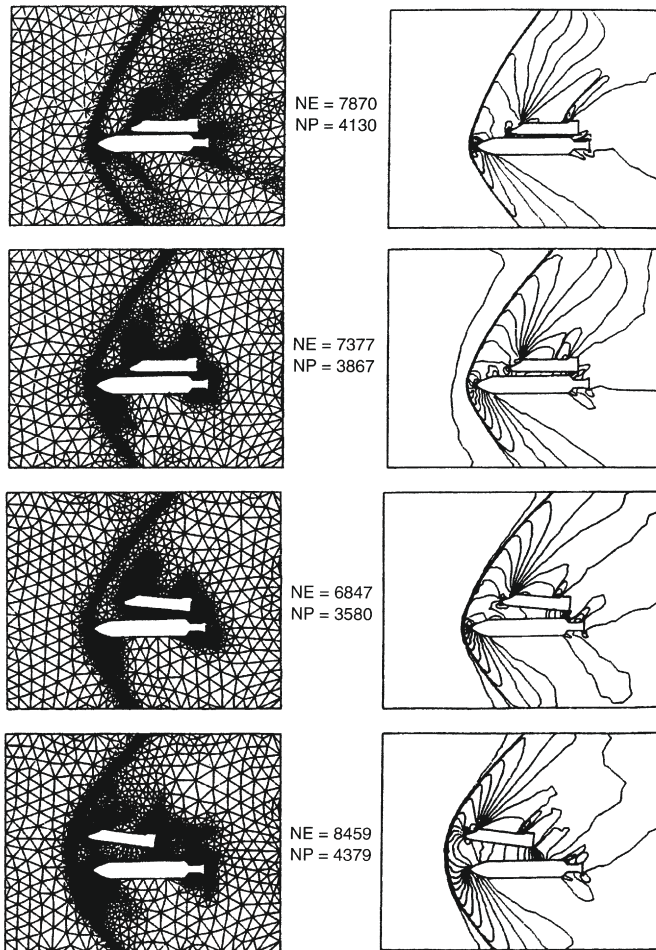
Supersonic car, THRUST SSC [35] comparison of finite element and experimental results.

**FIGURE 7.27**

A transient problem with adaptive remeshing [88]. Simulation of a sudden failure of a pressure vessel. Progression of refinement and velocity patterns shown. Initial mesh 518 nodes.

Example 7.12. Shuttle launch

A similar computation is shown in Fig. 7.28 where a diagrammatic form of a shuttle launch is modeled again as a two-dimensional problem [88]. Of course this two-dimensional model is purely imaginary but it is useful for showing the general configuration. In Fig. 7.29 however, we show a three-dimensional shuttle

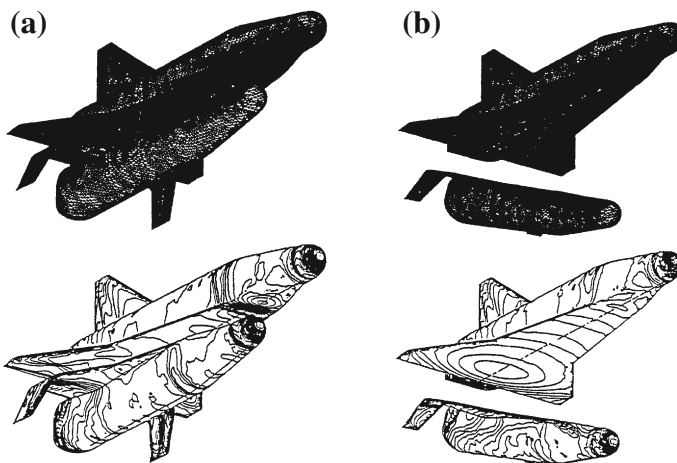
**FIGURE 7.28**

A transient problem with adaptive remeshing [88]. Model of the separation of shuttle and rocket. Mach 2, angle of attack -4° , initial mesh 4130 nodes.

approximating closely to reality [32]. The picture shows the initial configuration and the separation from the rocket.

7.11 Viscous problems in two dimensions

Clearly the same procedures which we have discussed previously could be used for the full Navier-Stokes equations by the introduction of viscous and other heat diffusion

**FIGURE 7.29**

Separation of a generic shuttle vehicle and rocket booster [32]. (a) Initial surface mesh and surface pressure; (b) final surface mesh and surface pressure.

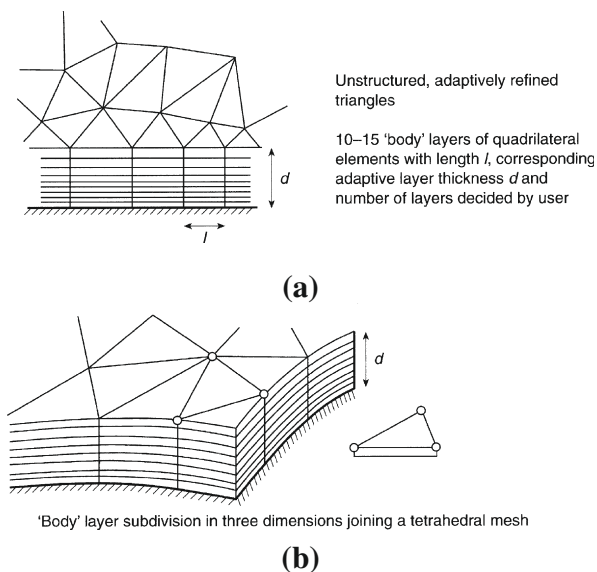
terms. Although this is possible we will note immediately that very rapid gradients of velocity will develop in the boundary layers (we have remarked on this already in Chapter 4) and thus special refinement will be needed there. In the first example we illustrate a viscous solution by using meshes designed *a priori* with fine subdivision near the boundary. However, in general the refinement must be done adaptively and here various methodologies of doing so exist. The simplest of course is the direct use of mesh refinement with elongated elements which we have also discussed in Chapter 4. This will be dealt with by a few examples in Section 7.11.1. However in Section 7.11.2 we shall address the question of much finer refinement with very elongated elements in the boundary layer. Generally we shall do such a refinement with a structured grid near the solid surfaces merging into the general unstructured meshing outside. In that section we shall introduce methods which can automatically separate structured and unstructured regions both in the boundary layer and in the shock regions.

The methodology is of course particularly important in problems of three dimensions.

The special refinement which we mentioned above is well illustrated in Fig. 7.30. In this we show the possibility of using a structured mesh with quadrilaterals in the boundary layer domain (for two-dimensional problems) and a three-dimensional equivalent of such a structured mesh using prismatic elements. Indeed such elements have been used as a general tool by some investigators [89–91].

Example 7.13. Viscous flow past a plate

The example given here is that in which both shock and boundary layer development occur simultaneously in high-speed flow over a flat plate [92]. This problem

**FIGURE 7.30**

Refinement in the boundary layer: (a) a two-dimensional sublayer of structured quadrilaterals; (b) a three-dimensional sublayer of prismatic elements.

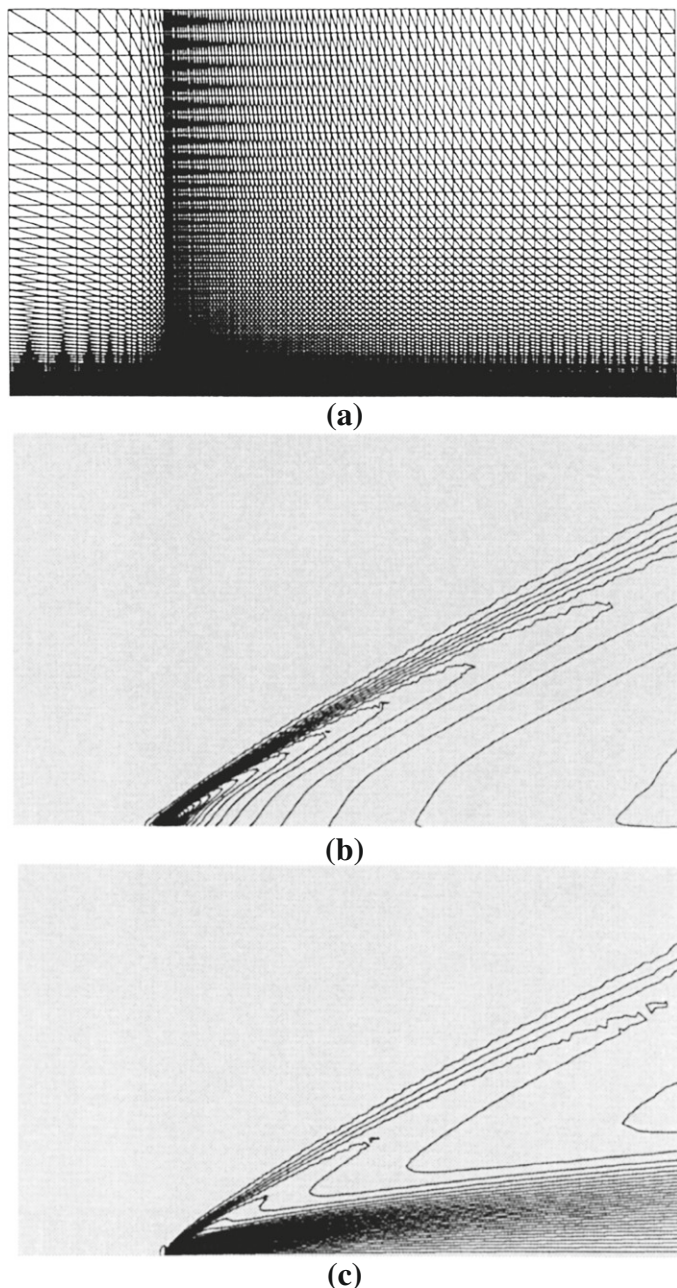
was studied extensively by Carter [93]. His finite difference solution is often used for comparison purposes although some oscillations can be seen.

A fixed mesh which is graded from a rather fine subdivision near the boundary to a coarser one elsewhere is shown in Fig. 7.31. We obtained the solution using the CBS algorithm. In Fig. 7.32, comparisons with Carter's [93] solution are presented and it will be noted that the CBS solution appears to be more consistent, avoiding oscillations near the leading edge.

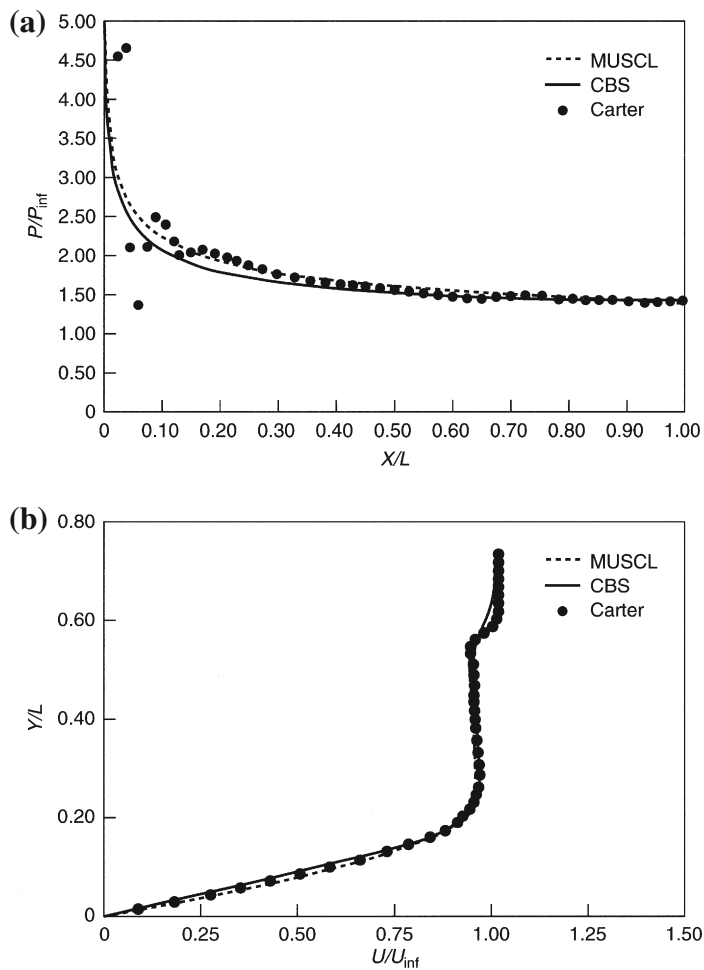
7.11.1 Adaptive refinement in both shock and boundary layer

In this section we shall pursue mesh generation and adaptivity in precisely the same manner as we have done in Chapter 4 and previously in this chapter, i.e., using elongated finite elements in the zones where rapid variation of curvature occurs. An example of this application is given in Fig. 7.33. Here now a problem of the interaction of a boundary layer generated by a flat plate and externally impinging shock is presented [94]. In this problem, some structured layers are used near the wall in addition to the direct approach of Chapter 4. The reader will note the progressive refinement in the critical area.

In such a problem it would be simpler to refine near the boundary or indeed at the shock using structured meshes and the idea of introducing such refinement is explored in the next section.

**FIGURE 7.31**

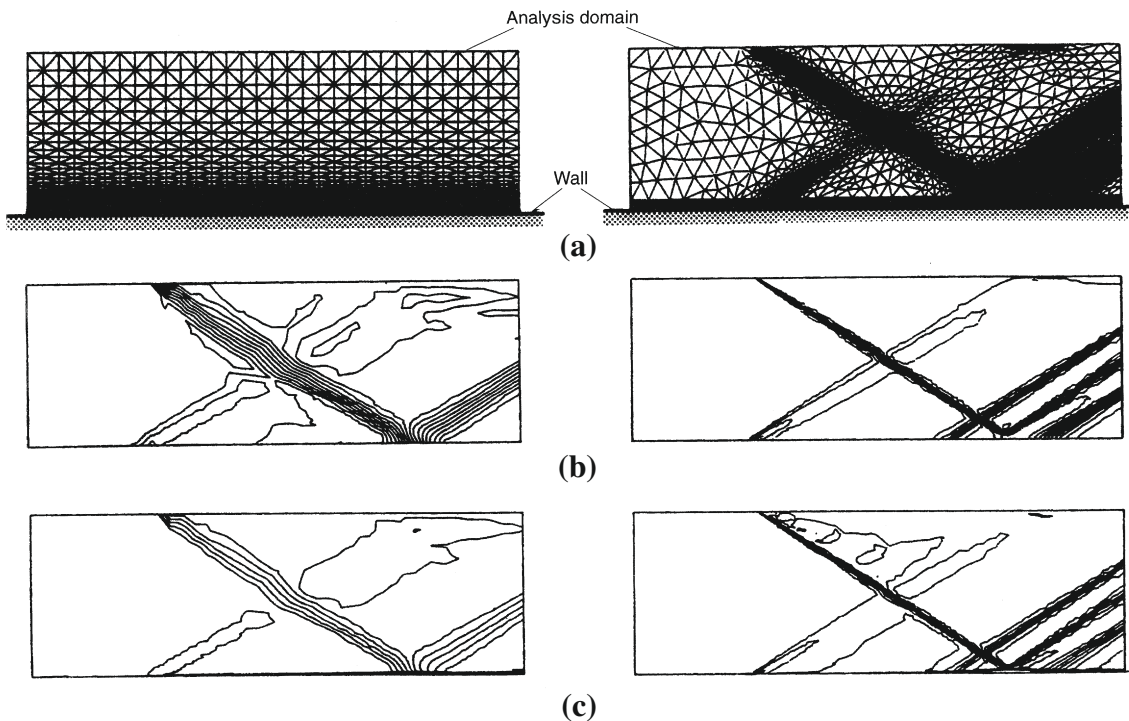
Viscous flow past a flat plate (Carter problem) [92]. Mach 3, $Re = 1000$. (a) Mesh, nodes: 6750, elements: 13,172. Contours of (b) pressure and (c) Mach number.

**FIGURE 7.32**

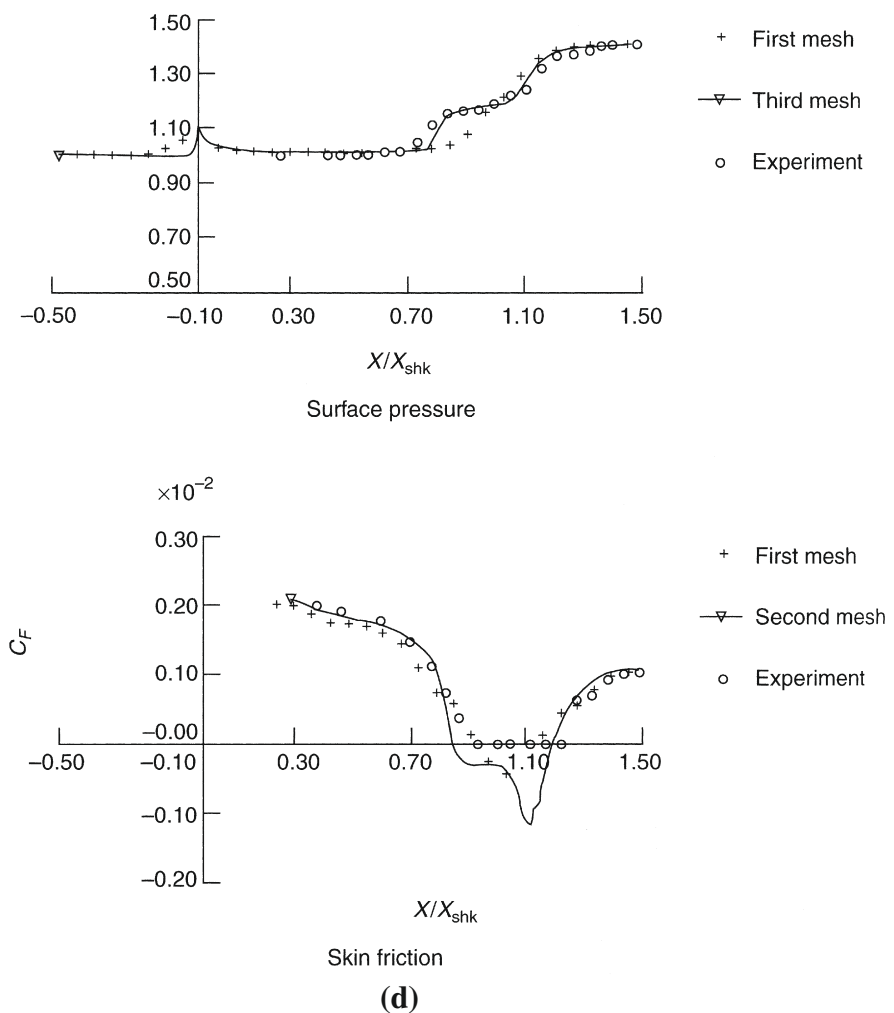
Viscous flow past a flat plate (Carter problem) [92]. Mach 3, $Re = 1000$. (a) Pressure distribution along the plate surface, (b) exit velocity profile.

7.11.2 Special adaptive refinement for boundary layers and shocks

As with the direct iterative approach, it is difficult to arrive at large elongations during mesh generation, and the procedures just described tend to be inaccurate. For this reason it is useful to introduce a structured layer within the vicinity of solid boundaries to model the boundary layers and indeed it is possible to do the same in the shocks

**FIGURE 7.33**

Shock and boundary layer interaction [94]. Final mesh, nodes: 4198. (a) Initial and final (second) adapted mesh; (b) initial and final (second) pressure contours; (c) initial and final (second) Mach number contours; (d) surface pressure and skin tension.

**FIGURE 7.33**

(Continued).

once these are defined. Within the boundary layer this can be done readily as shown in Fig. 7.30 using a layer of structured triangles or indeed quadrilaterals. On many occasions triangles have been used here to avoid the use of two kinds of elements in the same code. However if possible it is better to use directly quadrilaterals. The same problem can of course be done three dimensionally and we shall in Section 7.12 discuss application of such layers. Again in the structured layer we can use either prismatic

elements or simply tetrahedra though if the latter are used many more elements are necessary for the same accuracy. It is clear that unless the structured meshes near the boundary are specified *a priori*, an adaptive procedure will be somewhat complicated and on several occasions fixed boundary meshes have been used. However alternatives exist and here two possibilities should be mentioned. The first possibility, and that which has not yet been fully exploited, is that of refinement in which structured meshes are used in both shocks and boundary layers and the width of the domains is determined after some iterations. The procedure is somewhat involved and has been used with success in many trial problems as shown by Zienkiewicz and Wu [95]. We shall not describe the method in detail here but essentially structured meshes again composed of triangles or at least quadrilaterals divided into two triangles were used near the boundary and in the shock regions. In the second method we could imagine that normals are created on the boundaries, and a boundary layer thickness is predicted using some form of boundary layer analytical computation [25, 33, 96]. Within this layer structured meshes are adopted using a geometrical progression of thickness. The structured boundary layer meshing can of course be terminated where its need is less apparent and unstructured meshes continued outside.

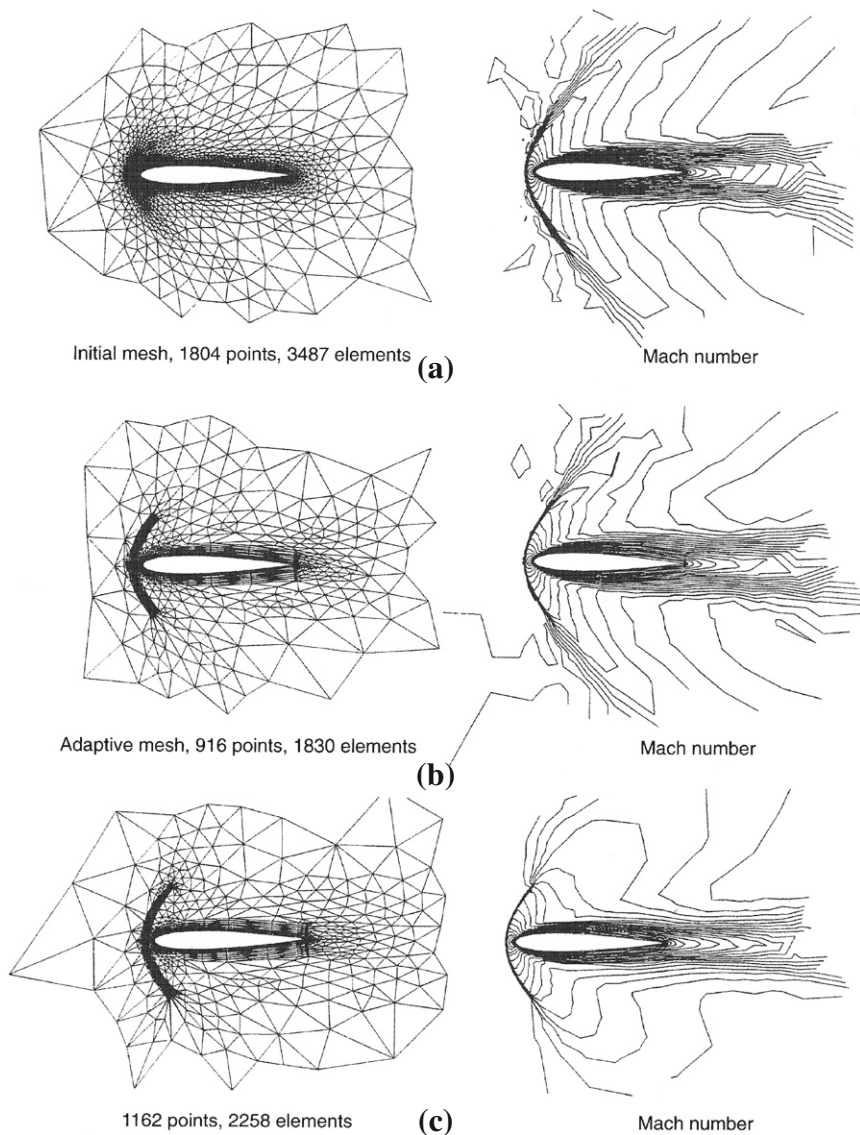
Figure 7.34 illustrates supersonic flow around an NACA0012 aerofoil using the automatic generation of structured and unstructured domains taken from Ref. [95]. The second method, in which normals are grown from the solid surface to create a structured layer, is illustrated in Fig. 7.35 on a two-component aerofoil.

Example 7.14. Transonic viscous flow past a NACA0012 aerofoil

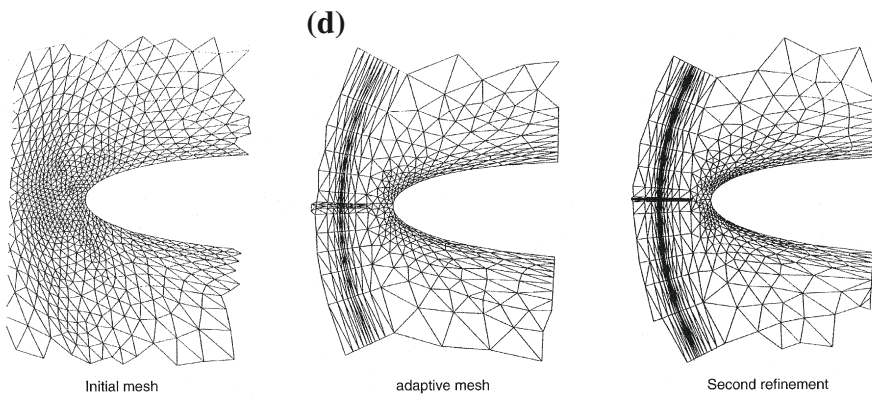
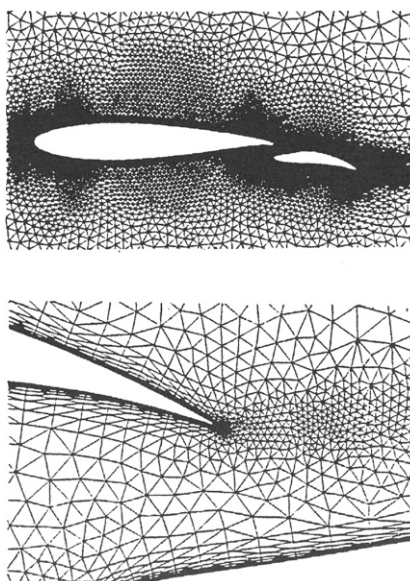
The external flow past a NACA0012 aerofoil is one of the popular benchmark problems of compressible fluid dynamics [97–99]. The transonic viscous flow is especially difficult to handle with many numerical schemes. The explicit schemes are generally difficult to use without additional acceleration procedures such as multigrid methods. Here, however we provide a solution using the explicit scheme without any additional acceleration technique. The problem consists of a NACA0012 aerofoil placed at the center of a circular domain of diameter 20 times the chord length. The inlet Mach number was assumed to be 0.85 and the Reynolds number was 2000. On the solid wall the no-slip conditions were assumed. The angle of attack in this problem was assumed to be zero. All the inlet conditions were assumed to be known.

In Figure 7.36 we show the mesh used for the calculations. As shown the mesh close to the solid wall is generated by constructing structured layers. Away from the wall the mesh is purely unstructured. This way we will be able to capture the strong boundary layer effects close to the walls. A total of 16,496 elements and 8425 nodes were employed in the calculation.

Figure 7.37 shows the Mach contours. In Figure 7.38 we show the surface quantity distribution. The quantity distribution in general is in excellent agreement with the fully structured mesh solutions [97–99].

**FIGURE 7.34**

Hybrid mesh for supersonic viscous flow past a NACA0012 aerofoil [95], Mach 2, and contours of Mach number: (a) initial mesh; (b) first adapted mesh; (c) final mesh; (d) mesh near stagnation point (shown opposite).

**FIGURE 7.34***(Continued).***FIGURE 7.35**

Structured grid in boundary layer for a two-component aerofoil [25]. Advancing boundary normals.

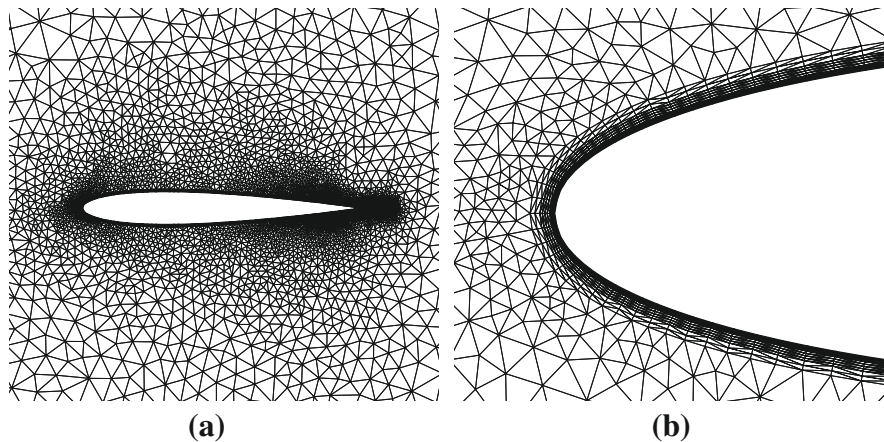


FIGURE 7.36

Transonic viscous flow past a NACA0012 aerofoil. Mach number 0.85, Reynolds number = 2000. (a) Finite element mesh; (b) structured layers close to the wall.

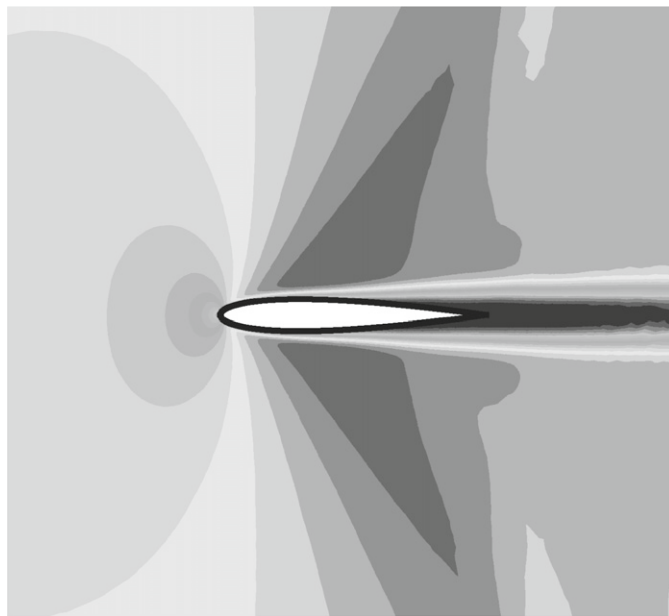
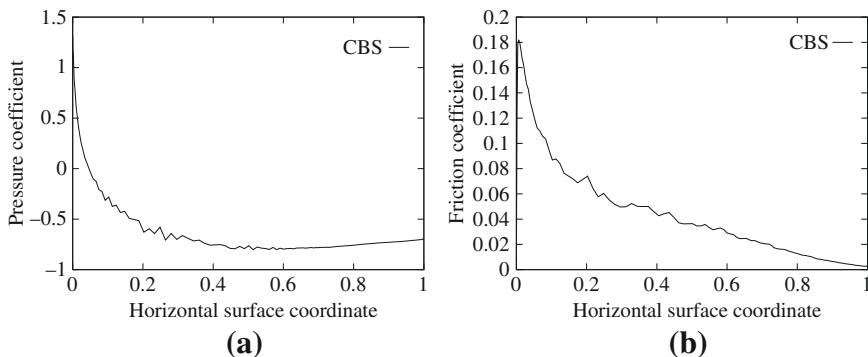


FIGURE 7.37

Transonic viscous flow past a NACA0012 aerofoil. Mach number 0.85, Reynolds number = 2000. Mach contours.

**FIGURE 7.38**

Transonic viscous flow past a NACA0012 aerofoil. Mach number 0.85, Reynolds number = 2000. (a) Surface pressure and (b) friction coefficients distribution.

7.12 Three-dimensional viscous problems

The same procedures which we have described in the previous section can of course be used in three dimensions. Quite realistic high Reynolds number boundary layers were so modeled. Figure 7.39 shows the mesh employed to solve viscous flow at a very high Reynolds number around a fore body of a double ellipsoid [25]. In this example a structured boundary layer is assumed *a priori*. The density contours are shown in Fig. 7.40.

7.13 Boundary layer: Inviscid Euler solution coupling

It is well known that high-speed flows which exist without substantial flow separation develop a fairly thin boundary layer to which all the viscous effects are confined. The flow outside this boundary layer is purely inviscid. Such problems have for some years been solved approximately by using pure Euler solutions from which the pressure distribution is obtained. Coupling these solutions with a boundary layer approximation written for a very small thickness near the solid body provides the complete solution. The theory by which the separation between inviscid and viscous domains is predicted is that based on the work of Prandtl and for which much development has taken place since his original work. Clearly various methods of solving boundary layer problems can be used and many different techniques of inviscid solution can be implemented.

In the boundary layer full Navier-Stokes equations are used and generally these equations are specialized by introducing the assumptions of a boundary layer in which no pressure variation across the thickness occurs.

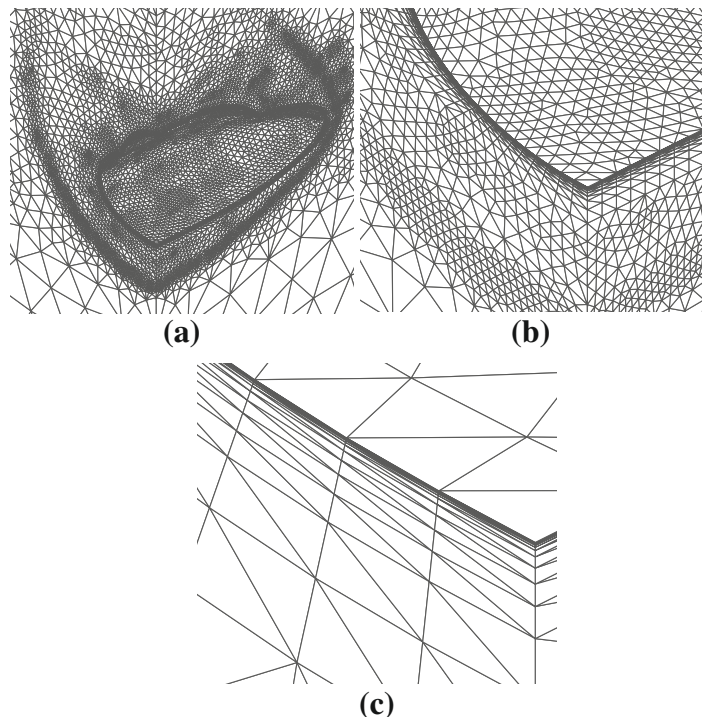


FIGURE 7.39

Hypersonic viscous flow past a double ellipsoid. Unstructured mesh with structured mesh layers close to the walls: (a) adapted mesh; (b) structured layers close to the wall; (c) close-up of structured layers.

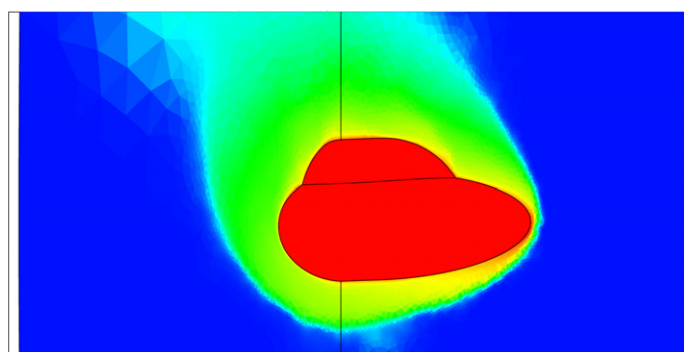


FIGURE 7.40

Hypersonic viscous flow past a double ellipsoid. Density contours.

An alternative to solving the equations in the whole boundary layer is the integral approach in which the boundary layer equations need to be solved only close to the solid surface. Here the “transpiration velocity model” for laminar flows [100] and the “lag-entrainment” method [101] for turbulent flows are notable approaches. Further extensions of these procedures can be found in many available research articles [102–106].

Many studies illustrate further developments and implementation procedures of viscous-inviscid coupling [107–109]. Although the use of such viscous-inviscid coupling is not directly applicable in problems where boundary layer separation occurs, many studies are available to deal with separated flows [110–112].

7.14 Concluding remarks

This chapter describes the most important and far-reaching possibilities of finite element application in the design of aircraft and other high-speed vehicles. The solution techniques described and examples presented illustrate that the possibility of realistic results exists. However, we do admit that there are still many unsolved problems. Most of these refer to either the techniques used for solving the equations or to modeling satisfactorily viscous and turbulence effects. The paths taken for simplifying and more efficient calculations have been outlined previously and we have mentioned possibilities such as multigrid methods, edge formulation, etc., designed to achieve faster convergence of numerical solutions. However full modeling of boundary layer effects is much more difficult, especially for high-speed flows. Use of boundary layer theory and turbulence models is of course only an approximation and here it must be stated that much “engineering art” has been used to achieve acceptable results. This inside knowledge is acquired from the use of data available from experiments and becomes necessary whether the turbulence models of any type are used or whether boundary layer theories are applied directly. In either case the freedom of choice is given to the user who will decide which model is satisfactory and which is not. For this reason the subject departs from being a precise mathematical science. The only possibility for such a science exists in direct turbulence modeling. Here of course only the Navier-Stokes equations which we have previously described are solved in a transient state when steady-state solutions do not exist. Doing this may involve billions of elements and at the moment is out of reach. We anticipate however that within the near future both computers and the methods of solution will be developed to such an extent that such direct approaches will become a standard procedure. At that time this chapter will serve purely as an introduction to the essential formulation possibilities. One aspect which can be visualized is that realistic three-dimensional turbulent computations will only be used in regions where these effects are important, leaving the rest to simpler Eulerian flow modeling. However the computational procedure which we are all striving for must be automatic and the formulation must be such that all choices made in the computation are predictable rather than imposed.

References

- [1] R. Löhner, K. Morgan, O.C. Zienkiewicz, The solution of non-linear hyperbolic equation systems by the finite element method, *Int. J. Numer. Methods Fluids* 4 (1984) 1043–1063.
- [2] R. Löhner, K. Morgan, O.C. Zienkiewicz, The use of domain splitting with an explicit hyperbolic solver, *Comput. Methods Appl. Mech. Eng.* 45 (1984) 313–329.
- [3] O.C. Zienkiewicz, K. Morgan, J. Peraire, M. Vahdati, R. Löhner, Finite elements for compressible gas flow and similar systems, in: *Seventh International Conference in Computational Methods in Applied Sciences and Engineering*, Versailles, December, 1985.
- [4] O.C. Zienkiewicz, R. Löhner, K. Morgan, J. Peraire, High speed compressible flow and other advection dominated problems of fluid mechanics, in: R.H. Gallagher, G.F. Carey, J.T. Oden, O.C. Zienkiewicz (Eds.), *Finite Elements in Fluids*, vol. 6, John Wiley, Chichester, 1985, pp. 41–88.
- [5] R. Löhner, K. Morgan, O.C. Zienkiewicz, An adaptive finite element procedure for compressible high speed flows, *Comput. Methods Appl. Mech. Eng.* 51 (1985) 441–465.
- [6] R. Löhner, K. Morgan, J. Peraire, O.C. Zienkiewicz, Finite element methods for high speed flows, AIAA paper 85–1531-CP, 1985.
- [7] J. Peraire, A finite method for convection dominated flows, Ph.D. Thesis, University of Wales, Swansea, Swansea, 1986.
- [8] R. Löhner, K. Morgan, J. Peraire, O.C. Zienkiewicz, L. Kong, Finite element methods for compressible flow, in: K.W. Morton, M.J. Baines (Eds.), *Numerical Methods in Fluid Dynamics*, vol. II, Clarendon Press, Oxford, 1986, pp. 27–52.
- [9] R. Löhner, K. Morgan, O.C. Zienkiewicz, Adaptive grid refinement for the Euler and compressible Navier-Stokes equations, in: I. Babuška, O.C. Zienkiewicz, J. Gago, E.R. de A. Oliveira (Eds.), *Accuracy Estimates and Adaptive Refinement in Finite Element Computations*, John Wiley & Sons, New York, 1986, pp. 281–298, (Chapter 15).
- [10] R. Löhner, K. Morgan, J. Peraire, M. Vahdati, Finite element, flux corrected transport (FEM–FCT) for the Euler and Navier–Stokes equations, *Int. J. Numer. Methods Fluids* 7 (1987) 1093–1109.
- [11] J. Peraire, M. Vahdati, K. Morgan, O.C. Zienkiewicz, Adaptive remeshing for compressible flow computations, *J. Comput. Phys.* 72 (1987) 449–466.
- [12] J. Peraire, K. Morgan, O.C. Zienkiewicz, Convection dominated problems, *Numerical Methods for Compressible Flows – Finite Difference, Element and Volume Techniques*, vol. AMD 78, ASME, New York, 1987, pp. 129–147.
- [13] R. Löhner, The efficient simulation of strongly unsteady flows by the finite element method, in: *25th Aerospace Science Meeting*, Reno, Nevada, 1987, AIAA Paper 87–0555.

- [14] J. Peraire, K. Morgan, J. Peiro, O.C. Zienkiewicz, An adaptive finite element method for high speed flows, in: AIAA 26th Aerospace Sciences Meeting, Reno, NV, 1987, Paper AIAA-87-0558.
- [15] O.C. Zienkiewicz, J.Z. Zhu, Y.C. Liu, K. Morgan, J. Peraire, Error estimates and adaptivity. From elasticity to high speed compressible flow, in: J. Whiteman (Ed.), *The Mathematics of Finite Elements and Applications*, vol. VII, Academic Press, London, 1988, pp. 483–512.
- [16] L. Formaggia, J. Peraire, K. Morgan, Simulation of state separation using the finite element method, *Appl. Math. Modelling* 12 (1988) 175–181.
- [17] O.C. Zienkiewicz, K. Morgan, J. Peraire, J. Peiro, L. Formaggia, Finite elements in fluid mechanics: compressible flow, shallow water equations and transport, ASME Conference on Recent Developments in Fluid Dynamics, vol. AMD 95, ASME, New York, December 1988.
- [18] J. Peraire, J. Peiro, L. Formaggio, K. Morgan, O.C. Zienkiewicz, Finite element Euler computations in three dimensions, *Int. J. Numer. Methods Eng.* 26 (1988) 2135–2159.
- [19] R.R. Thareja, J.R. Stewart, O. Hassan, K. Morgan, J. Peraire, A point implicit unstructured grid solver for the Euler and Navier–Stokes equation, *Int. J. Num. Meth. Fluids* 9 (1989) 405–425.
- [20] R. Löhner, Adaptive remeshing for transient problems, *Comput. Methods Appl. Mech. Eng.* 75 (1989) 195–214.
- [21] O. Hassan, K. Morgan, J. Peraire, An implicit–explicit scheme for compressible viscous high speed flows, *Comp. Meth. Appl. Mech. Eng.* 76 (1989) 245–258.
- [22] E.J. Probert, O. Hassan, K. Morgan, J. Peraire, An adaptive finite element method for transient compressible flows with moving boundaries, *Int. J. Numer. Methods Eng.* 32 (1991) 751–765.
- [23] E.J. Probert, O. Hassan, K. Morgan, J. Peraire, Adaptive explicit and implicit finite element methods for transient thermal analysis, *Int. J. Numer. Methods Eng.* 35 (1992) 655–670.
- [24] M.T. Manzari, P.R.M. Lyra, K. Morgan, J. Peraire, An unstructured grid FEM/MUSCL algorithm for the compressible Euler equations, in: Proceedings of the Eighth International Conference on Finite Elements in Fluids. New Trends and Applications, Pineridge Press, Swansea, 1993, pp. 379–388.
- [25] O. Hassan, E.J. Probert, K. Morgan, J. Peraire, Mesh generation and adaptivity for the solution of compressible viscous high speed flows, *Int. J. Numer. Methods Eng.* 38 (1995) 1123–1148.
- [26] P.R.M. Lyra, M.T. Manzari, K. Morgan, O. Hassan, J. Peraire, Upwind side based unstructured grid algorithms for compressible viscous flow computations, *Int. J. Eng. Anal. Des.* 2 (1995) 197–211.
- [27] O. Hassan, K. Morgan, E.J. Probert, J. Peraire, Unstructured tetrahedral mesh generation for three dimensional viscous flows, *Int. J. Numer. Methods Eng.* 39 (1996) 549–567.

- [28] M.T. Manzari, O. Hassan, K. Morgan, N.P. Weatherill, Turbulent flow computations on 3D unstructured grids, *Finite Elements Anal. Des.* 30 (1998) 353–363.
- [29] J.R. Stewart, T.J.R. Hughes, A tutorial in elementary finite element error analysis: A systematic presentation of a *priori* and a *posteriori* error estimates, *Comput. Methods Appl. Mech. Eng.* 158 (1–2) (1998) 1–22.
- [30] K. Morgan, J. Peraire, Unstructured grid finite element methods for fluid mechanics, *Rep. Prog. Phys.* 61 (1998) 569–638.
- [31] K. Morgan, P.J. Brookes, O. Hassan, N.P. Weatherill, Parallel processing for the simulation of problems involving scattering of electromagnetic waves, *Comput. Methods Appl. Mech. Eng.* 152 (1998) 157–174.
- [32] O. Hassan, L.B. Bayne, K. Morgan, N.P. Weatherill, An adaptive unstructured mesh method for transient flows involving moving boundaries, *ECCOMAS '98*, Wiley, New York, 1998.
- [33] O. Hassan, E.J. Probert, K. Morgan, Unstructured mesh procedures for the simulation of three dimensional transient compressible inviscid flows with moving boundary components, *Int. J. Num. Meth. Fluids* 27 (1998) 41–55.
- [34] N.P. Weatherill, E.A. Turner-Smith, J. Jones, K. Morgan, O. Hassan, An integrated software environment for multi-disciplinary computational engineering, *Eng. Comput.* 16 (1999) 913–933.
- [35] R. Ayers, O. Hassan, K. Morgan, N.P. Weatherill, The role of computational fluid dynamics in the design of the thrust supersonic car, *Design Optim. Int. J. Prod. & Proc. Improvement* 1 (1999) 79–99.
- [36] K. Morgan, O. Hassan, N.P. Weatherill, Why didn't the supersonic car fly? *Mathematics Today. Bull. Inst. Math. Appl.* 35 (Aug 1999) 110–114.
- [37] K. Morgan, N.P. Weatherill, O. Hassan, P.J. Brookes, R. Said, J. Jones, A parallel framework for multidisciplinary aerospace engineering simulations using unstructured meshes, *Int. J. Num. Meth. Fluids* 31 (1999) 159–173.
- [38] R. Said, N.P. Weatherill, K. Morgan, N.A. Verhoeven, Distributed parallel Delaunay mesh generation, *Comp. Meth. Appl. Mech. Eng.* 177 (1999) 109–125.
- [39] P.M.R. Lyra, K. Morgan, A review and comparative study of upwind biased schemes for compressible flow computation. Part I: 1-D first-order schemes, *Arch. Comp. Meth. Eng.* 7 (2000) 19–55.
- [40] K.A. Sorensen, O. Hassan, K. Morgan, N.P. Weatherill, Agglomerated multigrid on hybrid unstructured meshes for compressible flow, *Int. J. Numer. Methods Fluids* 40 (2002) 593–603.
- [41] K.A. Sorensen, O. Hassan, K. Morgan, N.P. Weatherill, A multigrid accelerated time-accurate inviscid compressible fluid flow solution algorithm employing mesh movement and local remeshing, *Int. J. Numer. Methods Fluids* 43 (2003) 517–536.
- [42] K.A. Sorensen, O. Hassan, K. Morgan, N.P. Weatherill, A multigrid accelerated hybrid unstructured mesh method for 3D compressible turbulent flow, *Comput. Mech.* 31 (2003) 101–114.

- [43] O. Hassan, K.A. Sorensen, K. Morgan, N.P. Weatherill, A method for time accurate turbulent compressible fluid flow simulation with moving boundary components employing local remeshing, *Int. J. Numer. Methods Fluids* 53 (8) (March 20 2007) 1243–1266, 13th International Conference on Finite Elements for Flow Problems, Swansea, Wales, 04–06 April 2005.
- [44] R. Löhner, H. Luo, J.D. Baum, D. Rice, Improvements in speed for explicit, transient compressible flow solvers, *Int. J. Numer. Methods Fluids* 56 (12) (2008) 2229–2244, APR 30.
- [45] O. Hassan, K. Morgan, N.P. Weatherill, Unstructured mesh methods for the solution of the unsteady compressible flow equations with moving boundary components, *Philos. Trans. Roy. Soc. A - Math. Phys. Eng. Sci.* 365 (1859) (2007) 2531–2552, October 15.
- [46] O. Hassan, K. Morgan, Fully parallel environment, for the simulation of unsteady flow with moving boundary components, in: B.H.V. Topping, P. Ivanyi (Eds.), *Parallel, Distributed and Grid Computing for Engineering, Computational Science Engineering and Technology Series*, vol. 21, Univ Pecs, Pollack Mihaly Fac Engn, Pecs, Hungary, 2009, pp. 1–20, First International Conference on Parallel, Distributed and Grid Computing for Engineering, 06–08 April 2009.
- [47] B.J. Evans, O. Hassan, J.W. Jones, K. Morgan, L. Remaki, Computational fluid dynamics applied to the aerodynamic design of a land-based supersonic vehicle, *Numer. Methods Part. D. E.* 27 (1, SI) (JAN 2011) 141–159, Conference on Mathematics of Finite Elements and Applications, London, England, 09–12 June 2009.
- [48] R. Sevilla, O. Hassan, K. Morgan, An analysis of the performance of a high-order stabilised finite element method for simulating compressible flows, *Comput. Methods Appl. Mech. Eng.* 253 (2013) 15–27.
- [49] C. Hirsch, *Numerical computation of internal and external flows, Fundamentals of Numerical Discretization*, vol. I, John Wiley & Sons, Chichester, 1988.
- [50] L. Demkowicz, J.T. Oden, W. Rachowicz, A new finite element method for solving compressible Navier-Stokes equations based on an operator splitting method and $h\text{-}p$ adaptivity, *Comput. Methods Appl. Mech. Eng.* 84 (1990) 275–326.
- [51] C. Hirsch, *Numerical computation of internal and external flows: II Computational method for inviscid and viscous flows*, in: *Wiley Series in Numerical Methods in Engineering*, John Wiley and Sons, Chichester, UK, 1990.
- [52] J. Vadyak, J.D. Hoffman, A.R. Bishop, Flow computations in inlets at incidence using a shock fitting bicharacteristic method, *AIAA J.* 18 (1980) 1495–1502.
- [53] K.W. Morton, M.F. Paisley, A finite volume scheme with shock fitting for steady Euler equations, *J. Comput. Phys.* 80 (1989) 168–203.
- [54] J. von Neumann, R.D. Richtmyer, A method for the numerical calculations of hydrodynamical shocks, *J. Math. Phys.* 21 (1950) 232–237.
- [55] A. Lapidus, A detached shock calculation by second order finite differences, *J. Comp. Phys.* 2 (1967) 154–177.

- [56] J.L. Steger, Implicit finite difference simulation of flow about two dimensional geometries, *AIAA J.* 16 (1978) 679–686.
- [57] R.W. MacCormack, B.S. Baldwin, A numerical method for solving the Navier–Stokes equations with application to shock boundary layer interaction, Paper AIAA-75-1, 1975.
- [58] A. Jameson, W. Schmidt, Some recent developments in numerical methods in transonic flows, *Comp. Meth. Appl. Mech. Eng.* 51 (1985) 467–493.
- [59] K. Morgan, J. Peraire, J. Peiro, O.C. Zienkiewicz, Adaptive remeshing applied to the solution of a shock interaction problem on a cylindrical leading edge, in: P. Stow (Ed.), *Computational Methods in Aeronautical Fluid Dynamics*, Clarendon Press, Oxford, 1990, pp. 327–344.
- [60] R. Codina, A discontinuity capturing crosswind-dissipation for the finite element solution of convection diffusion equation, *Comput. Methods Appl. Mech. Eng.* 110 (1993) 325–342.
- [61] P. Nithiarasu, O.C. Zienkiewicz, B.V.K.S. Sai, K. Morgan, R. Codina, M. Vázquez, Shock capturing viscosities for the general fluid mechanics algorithm, *Int. J. Num. Meth. Fluids* 28 (1998) 1325–1353.
- [62] T.J.R. Hughes, M. Malett, A new finite element formulation for fluid dynamics. Part IV: A discontinuity capturing operator for multidimensional advective–diffusive problems, *Comp. Mech. Appl. Mech. Eng.* 58 (1986) 329–336.
- [63] C. Johnson, A. Szepessy, On convergence of a finite element method for a nonlinear hyperbolic conservation law, *Math. Comput.* 49 (1987) 427–444.
- [64] A.C. Galeão, E.G. Dutra Do Carmo, A consistent approximate upwind Petrov–Galerkin method for convection dominated problems, *Comp. Meth. Appl. Mech. Eng.* 68 (1988) 83–95.
- [65] P. Hansbo, C. Johnson, Adaptive streamline diffusion methods for compressible flow using conservation variables, *Comp. Meth. Appl. Mech. Eng.* 87 (1991) 267–280.
- [66] F. Shakib, T.R.J. Hughes, Z. Johan, A new finite element formulation for computational fluid dynamics: Part X. The compressible Euler and Navier–Stokes equations, *Comput. Methods Appl. Mech. Eng.* 89 (1991) 141–219.
- [67] P. Nithiarasu, O.C. Zienkiewicz, B.V.K.S. Sai, K. Morgan, R. Codina, M. Vázquez, Shock capturing viscosities for the general algorithm, in: M. Hafez, J.C. Heinrich (Eds.), *Tenth International Conference on Finite Elements in Fluids*, 5–8 January, Tucson, Arizona, USA, 1998, pp. 350–356.
- [68] C.G. Thomas, P. Nithiarasu, Influences of element size and variable smoothing on inviscid compressible flow solution, *Int. J. Numer. Methods Heat Fluid Flow* 15 (5–6) (2005) 420–428.
- [69] G. Sod, A survey of several finite difference methods for systems of non-linear hyperbolic conservation laws, *J. Comput. Phys.* 27 (1978) 1–31.

- [70] T.E. Tezduyar, T.J.R. Hughes, Finite element methods for first order hyperbolic systems with particular emphasis on the compressible Euler equation, *Comput. Methods Appl. Mech. Eng.* 45 (1984) 217–284.
- [71] P. Woodward, P. Colella, The numerical simulation of two dimensional flow with strong shocks, *J. Comput. Phys.* 54 (1984) 115–1173.
- [72] T.H. Pulliam, J.T. Barton, Euler computations of AGARD Working Group 07 airfoil test cases, in: AIAA-85-0018, AIAA 23rd Aerospace Sciences Meeting, 1985, 14–17 January.
- [73] O.C. Zienkiewicz, K. Morgan, J. Peraire, M. Vahdati, R. Löhner, Finite elements for compressible gas flow and similar systems, in: Seventh International Conference in Computational Methods in Applied Sciences and Engineering, Versailles, December 1985.
- [74] O.C. Zienkiewicz, J.Z. Zhu, A simple error estimator and adaptive procedure for practical engineering analysis, *Int. J. Numer. Methods Eng.* 24 (1987) 337–357.
- [75] J.T. Oden, L. Demkowicz, Advance in adaptive improvements: A survey of adaptive methods in computational fluid mechanics, in: A.K. Noor, J.T. Oden (Eds.), *State of the Art Survey in Computational Fluid Mechanics*, American Society of Mechanical Engineers, 1988.
- [76] P.R.M. Lyra, K. Morgan, J. Peraire, J. Peiro, TVD algorithms for the solution of compressible Euler equations on unstructured meshes, *Int. J. Num. Meth. Fluids* 19 (1994) 827–847.
- [77] J.R. Stewart, R.R. Thareja, A.R. Wieting, K. Morgan, Application of finite elements and remeshing techniques to shock interference on a cylindrical leading edge, Paper AIAA-88-0368, 1988.
- [78] R.A. Nicolaides, On finite element multigrid algorithms and their use, in: J.R. Whiteman (Ed.), *MAFELAP 1978, The Mathematics of Finite Elements and Applications III*, Academic Press, London, 1979, pp. 459–466.
- [79] W. Hackbusch, U. Trottenberg (Eds.), *Multigrid Methods*, Springer-Verlag, Berlin, 1982.
- [80] R. Löhner, K. Morgan, An unstructured multigrid method for elliptic problems, *Int. J. Numer. Methods Eng.* 24 (1987) 101–115.
- [81] M.C. Rivara, Local modification of meshes for adaptive and or multigrid finite element methods, *J. Comp. Appl. Math.* 36 (1991) 79–89.
- [82] S. Lopez, R. Casciaro, Algorithmic aspects of adaptive multigrid finite element analysis, *Int. J. Num. Meth. Eng.* 40 (1997) 919–936.
- [83] P. Wessling, *An Introduction to Multigrid Methods*, R.T. Edwards Inc., 2004.
- [84] J. Peraire, J. Peiro, L. Formaggia, K. Morgan, O.C. Zienkiewicz, Finite element Euler computations in 3-dimensions, *Int. J. Numer. Methods Eng.* 26 (1989) 2135–2159.
- [85] A. Jameson, T.J. Baker, N.P. Weatherill, Calculation of inviscid transonic flow over a complete aircraft, in: AIAA 24th Aerospace Science Meeting, Reno, Nevada, 1986, Paper AIAA-86-0103.

- [86] V. Billey, J. Periaux, P. Perrier, B. Stoufflet, 2D and 3D Euler computations with finite element methods in aerodynamics, *Lect. Notes Math.* 1270 (1987) 64–81.
- [87] R. Noble, *THRUST, The Remarkable Story of One Man's Quest for Speed*, Bantam, London, 1998.
- [88] E.J. Probert, Finite element method for convection dominated flows, Ph.D. Thesis, University of Wales, Swansea, 1986.
- [89] Y. Kallinderis, S. Ward, Prismatic grid generation for 3-dimensional complex geometries, *AIAA J.* 31 (1993) 1850–1856.
- [90] Y. Kallinderis, Adaptive hybrid prismatic tetrahedral grids, *Int. J. Num. Meth. Fluids* 20 (1995) 1023–1037.
- [91] A.J. Chen, Y. Kallinderis, Adaptive hybrid (prismatic-tetrahedral) grids for incompressible flows, *Int. J. Num. Meth. Fluids* 26 (1998) 1085–1105.
- [92] O.C. Zienkiewicz, P. Nithiarasu, R. Codina, M. Vazquez, P. Ortiz, The characteristic-based-split (CBS) procedure: An efficient and accurate algorithm for fluid problems, *Int. J. Numer. Methods Fluids* 31 (1999) 359–392.
- [93] J.E. Carter, Numerical solutions of the Navier–Stokes equations for the supersonic laminar flow over a two-dimensional compression corner, *NASA TR-R-385*, 1972.
- [94] O. Hassan, Finite element computations of high speed viscous compressible flows, Ph.D. Thesis, University of Wales, Swansea, 1990.
- [95] O.C. Zienkiewicz, J. Wu, Automatic directional refinement in adaptive analysis of compressible flows, *Int. J. Numer. Methods Eng.* 37 (1994) 2189–2219.
- [96] M.J. Castro-Diaz, H. Borouchaki, P.L. George, F. Hecht, B. Mohammadi, Anisotropic adaptive mesh generation in two dimensions for CFD, in: *Computational Fluid Dynamics '96*, 1996, pp. 181–186.
- [97] L. Cambier, Computation of viscous transonic flows using an unsteady type method and a zonal grid refinement technique, in: M.O. Bristrau, R. Glowinski, J. Periaux, H. Viviand (Eds.), *Numerical Simulation of Compressible Navier–Stokes Flows*, Notes of Numerical Fluid Mechanics, vol. 18, Vieweg, Wiesbaden, 1987.
- [98] N. Satofuka, K. Morinishi, Y. Nishida, Numerical simulation of two-dimensional compressible Navier–Stokes equations using rational Runge–Kutta method, in: M. OBristrau, R. Glowinski, J. Periaux, H. Viviand (Eds.), *Numerical Simulation of Compressible Navier–Stokes Flows*, Notes of Numerical Fluid Mechanics, vol. 18, Vieweg, Wiesbaden, 1987.
- [99] S. Mittal, Finite element computation of unsteady viscous compressible flows, *Comput. Methods Appl. Mech. Eng.* 157 (1998) 151–175.
- [100] M.J. Lighthill, On displacement thickness, *J. Fluid Mech.* 4 (1958) 383.
- [101] J.E. Green, D.J. Weeks, J.W.F. Brooman, Prediction of turbulent boundary layers and wakes in compressible flow by a lag-entrainment method, *Aeronautical Research Council Report and Memo Report No. 3791*, 1973.

- [102] P. Bradshaw, The analogy between streamline curvature and buoyancy in turbulent shear flow, *J. Fluid Mech.* 36 (1969) 177–191.
- [103] J.E. Green, The prediction of turbulent boundary layer development in compressible flow, *J. Fluid Mech.* 31 (1969) 753–778.
- [104] H.B. Squire, A.D. Young, The calculation of the profile drag of aerofoils, Aeronautical Research Council Repo. and Memo 1838, 1937.
- [105] R.E. Melnok, R.R. Chow, H.R. Mead, Theory of viscous transonic flow over airfoils at high Reynolds number, Paper AIAA-77-680, 1977.
- [106] J.C. Le Balleur, Calcul par copulage fort des écoulements visqueux transsoniques incluant sillages et décollemants. La Recherche Aerospatiale, Profils d'aile portant, May–June 1981.
- [107] J. Szmelter, A. Pagano, Viscous flow modelling using unstructured meshes for aeronautical applications, in: S.M. Deshpande et al. (Eds.), *Lecture Notes in Physics*, vol. 453, Springer-Verlag, Berlin, 1994.
- [108] J. Szmelter, Viscous coupling techniques using unstructured and multiblock meshes, ICAS Paper ICAS-96-1.7.5, Sorrento, 1996.
- [109] J. Szmelter, Aerodynamic wing optimisation. Paper AIAA-99-0550, 1999.
- [110] J.C. Le Balleur, Viscous–inviscid calculation of high lift separated compressible flows over airfoils and wings, in: Proceedings AGARD/FDP High Lift Aerodynamics, AGARD-CP515, Banff, Canada, 1992.
- [111] J.C. Le Balleur, Calculation of fully three-dimensional separated flows with an unsteady viscous–inviscid interaction method, in: Fifth International Symposium on Numerical and Physical Aspects of Aerodynamic Flows, Long Beach CA (USA), 1992.
- [112] J.C. Le Balleur, P. Girodroux-Lavigne, Calculation of dynamic stall by viscous–inviscid interaction over airfoils and helicopter-blade sections, in: AHS 51st Annual Forum and Technology Display, Fort Worth, TX USA, 1995.